

Running head: Trace Metals in Calcite

An Experimental Determination of the Incorporation of Trace Metals into Calcite

Maya Reimi Wendelbo

Washington and Lee University

*Para mis padres, por darme alas,
y para Morten, por ayudarme a volar.*

Acknowledgements

This research would not have been possible without the instrumental help of my faculty advisor Dr. Paul Low. The Washington and Lee Geology department provided the funding and all of the access to analytical equipment used in this work.

Table of Contents

Acknowledgements.....	3
Abstract	6
Introduction.....	7
Calcite.....	7
Incorporation.....	8
Trace Metals	12
Importance of a New Decontamination Method	15
Materials and Methods	18
Calcite Synthesis	18
Trace Metal Addition.....	19
X-Ray Diffraction Analysis	21
Inductive Coupled Plasma Optical Emission Spectroscopy	21
Mercury and the ICP-OES.....	22
Ion Chromatography	22
ICP-Mechanical Separation.....	23
Results.....	25
Optical Analysis.....	25
X-ray Diffraction	28
ICP – Trace Metals.....	29

Ion Chromatography.....	35
Partition Coefficients	38
Discussion.....	40
Partition Coefficients	43
Limitations to Implementation.....	44
Future Work.....	46
Conclusions	47
References	49

Abstract

A new experimental method to synthesize calcite crystals via aqueous slow diffusion was used to examine the level of incorporation of six different trace metal (Co, Mn, Pb, Hg, As, Se) contaminants in calcite. The aqueous reagent solutions had a constant pH and calcium concentrations and varied only in the concentrations of the trace metal contaminants. The experiments resulted in euhedral rhombohedral calcite crystals in the 100 μm range and up to 500 μm across. ICP-OES analysis of the trace metal solutions before and after the calcite precipitation indicated a large decrease in cobalt and manganese abundance at all trace metal concentrations, and in lead in the part-per-million concentrations; a modest decrease in the abundance of lead at low concentrations and mercury at high concentrations; and a small decrease in the abundance of selenium at all concentrations and mercury at low concentrations.

Introduction

Calcite

Calcite is stable polymorph of CaCO_3 , calcium carbonate, at surface temperature and pressure, and it accounts for the majority of rock forming carbonates. The calcite structure is fairly simple, divalent calcium is octahedrally coordinated to six oxygen ions each belonging to a different carbonate ion (Figure 1). The carbonate ion is a triangular arrangement of three carbon ions and one oxygen ion. In a hexagonal system layers of calcium and carbonate alternate along the c axis. This same structure is replicated in other anhydrous single carbonates including rhodochrosite (MnCO_3) and spherocobaltite (CoCO_3). Some single carbonates, like cerussite (PbCO_3), are instead 9-fold coordinated, where Pb is coordinated with eight oxygen atoms, due to its larger cation size (Reeder 1983b). Carbonates are vastly important in sedimentary rocks and have a long record of biological, physical and chemical interactions through geologic time (Reeder 1983a).

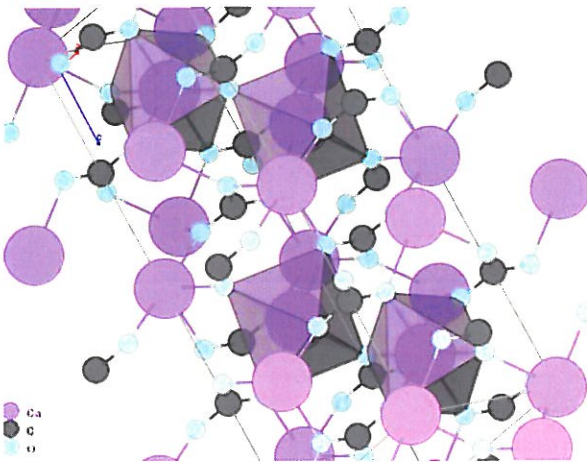


Figure 1: Calcite structure, shows the atomic bonds and coordination. The shaded octahedron shows coordination between Ca^{2+} and six oxygen atoms. Graft 1961 in <http://webmineral.com/data/Calcite.shtml>

Calcite has been used in the past for many sorption experiments because it is naturally abundant, geochemically relevant, and it grows in monomolecular planes with a well-defined lattice structure and surface chemistry. As calcite grows, molecular steps aligned with the four rhombohedral edges of the cleavage plane are the predominant surfaces for growth and dissolution processes, because of the simple steady advance of monomolecular steps calcite provides a heterogeneous reactive plane (Hay, Workman, & Manne, 2002). The rates of these reactions are often moderate in comparison with slow clay formation process and fast typical marine evaporative (Morse 1983). With varying pH and temperatures, the kinetics of calcite crystallization can be, either dominated by the transport rate or by the chemical reaction rate (Rickard & Sjöberg, 1983). For this synthesis method, the initial pH is set at 2.05-2.2, allowing the system to be dominated by transport rate. As the experiment progresses and the pH increases (Morrison, Reimi & Burns, "unpublished"), the reaction rates become chemically dominated. The precipitation reaction is part of an H⁺ dependent system. Some studies have found that the precipitation rates have a large effect on the coprecipitation of divalent cations with calcite (Lorens, 1981; Ohara and Reid, 1973; Curti, 1999). In our current system pH, and reaction rate are positively related, in that an increase of the pH of the initial solution would result in an increase in the calcite precipitation rate. The desired precipitation rate for this study is to fast enough to successfully synthesize calcite in several days, but slow enough to grow euhedral calcite crystals.


Incorporation

Cations can become incorporated into calcite in several mechanisms. The most prominent mechanism of incorporation is the substitution of a cation for Ca²⁺ (Veizer,

1983). This process is largely dependent on the ionic radius and charge of the substituting ion (Blundy and Wood, 2003). In the case of calcite, a divalent cation smaller than calcium can substitute for calcium in a solid solution series resulting in a different end member single carbonate mineral, like rhodonchrosite or spherocobaltite, which are calcite isomorphs. Ca^{2+} , with an ionic radius of 1.00 (Shannon, 1976), is near the size limit for six-fold coordination with oxygen, when some larger ions substitutive for calcium the end member of the solid solution is instead in eight-fold or 9-fold coordination with oxygen, like in the case of the lead -rich carbonate, cerussite (Reeder, 1983b).

If the charge of the substituting ion is different from the original ion (in this case if it is not divalent), then an electrostatic charge penalty needs to be paid (Blundy and Wood, 2003). Heterovalent substitution can work in two different ways, through a coupled substitution mechanism, when two different ions substitute in for Ca^{2+} and ensure a charge balance – for example one As^{3+} and one Na^{+} in place for two Ca^{2+} ions or through an omission substitution where in order to place a heterovalent ion you need to leave space in the crystal lattice empty –if you want to substitute one Se^{4+} for two Ca^{2+} leaving one lattice site empty. Se^{4+} can also bond with three oxygen atoms and replace a carbonate ion instead of trying to enter the calcite structure (Aurelio et. al, 2010). Omission substitution is different from the process of species that are trapped in lattice defect, because the ions become part of the crystal structure in specific lattice sites. Even neutral species, like noble gases, can be incorporated into the Ca^{2+} lattice site by paying a 4+ charge penalty (incorporate one He atom and two Th^{4+} ions instead of three Ca^{2+} ions), which means that neutral species behave like heterovalent cations for modeling proposes in incorporation studies (Brooker et al., 2003).

Work by Blundy and Wood (2003) to predict the partition coefficient for trace metals between the crystallization of silicate melt and clinopyroxene. Blundy and Wood (2003) based their model on the ideal that each crystal structure has an ideal lattice size and that there is kinetic work associated with the substitution of non ideal ions into a specific site, due to the fact that the lattice must be deformed in order to accommodate a larger or smaller than ideal cations. This concept of “lattice strain theory” was used by Blundy and Wood to predict coefficient of partition of trace metals in the octahedral M1 site that usually contains calcium in clinopyroxene (Equation 1). The M1 site in clinopyroxene, like in calcite, is an octahedrally coordinated site, for which calcium is assumed to be the ideal ionic size for the lattice parameter. The predicted K_D values were calculated using the ionic radius for octahedrally coordinated trace metals in this study as published by Shannon 1976 (Figure 2). Table 1 is a summary of the predicted compatibility levels for each element based on its ionic radius.



$$D_i = D_{0(M)}^{n+} \cdot \exp \left\{ \frac{-4\pi \cdot N_A \cdot E_M^{n+} \left[\frac{1}{2} r_{0(M)}^{n+} (r_i - r_{0(M)}^{n+})^2 + \frac{1}{3} (r_i - r_{0(M)}^{n+})^3 \right]}{RT} \right\}$$

Concentration of an ion with a particular charge in the melt
 Concentration of an ion with a particular charge in the mineral
 Avogadro's number
 Lattice strain parameter (Young's modulus)
 Radius of lattice site
 Radius of ion
 Temperature
 Noble gas constant

Equation 1: Prediction of the coefficient of partition of trace metals with a specific charge and size (Blundy and Wood, 2003)

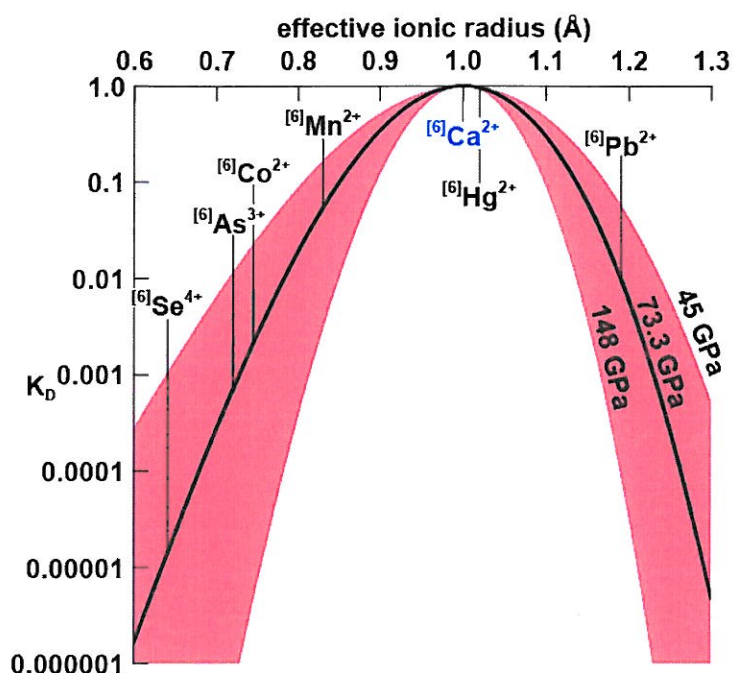


Figure 2: Solutions to Blundy and Wood (2003) based on the octahedral site in calcite, assuming that calcium is the ideal ion for the site. The shaded area is based on three different lattice strain parameters (Young's modulus) with the black line delimiting the median Young's modulus used.

Element	Ionic radii Shannon (1976)	charge	Predicted Compatibility
Hg ^[6]	1.02 Å	2+	High
Mn ^[6]	0.83 Å	2+	Medium
Pb ^[6]	1.19 Å	2+	Medium
Co ^[6]	0.745 Å	2+	Medium
As ^[6]	0.72 Å	3+	Poor
Se ^[6]	0.64 Å	4+	Poor

Table 1: Predicted compatibility for each trace metal based on its ionic radii and charge.

Some solid solution models are based on thermodynamic laws, and even though, in principle, they are correct they have limited real life applications, due to the fact that it is difficult to account for all of the processes that can occur simultaneously to crystallization. The current models can only predict isomorph solid solutions and fail to account for impure carbonate situations because they only account for incorporation based on one

specific lattice site (and not multiple precipitates), and cannot be expanded to include other incorporation mechanism (Curti, 1999). However solid solution models can provide a theoretical framework for the minimum expected compatibility of an ion in a specific lattice site.

Another incorporation mechanism that plays an important role in aqueous calcite processes is sorption. Sorption is a blanket term that encompasses several surface incorporation processes for the uptake of foreign ions by a solid phase, independent of the specific mechanism (Sposito, 1986; Zachara, 1991). The term sorption includes the, sometimes temporary, adsorption to the surface of a mineral due to remnant ionic charges, the chemisorption -chemical interaction with the surface or the eventual absorption into the bulk of the mineral via a solid-state diffusion (Hay, 2002). Sorption is a key process in controlling the mobility and availability of many aqueous contaminants (Sø et al., 2008).

In this experimental study, the metal contaminants can be potentially removed from their aqueous states by multiple mechanisms. They can be incorporated to calcite crystals through substitution for Ca^{2+} which would be constrained by lattice strain theory, or through sorption to the calcite surface post-crystallization. Contaminants can also precipitate in different minerals that are members of a calcium solid solution series, like rhodochrosite and other divalent metal end member minerals, like cerussite or spherocobaltite.

Trace Metals

This study aims to create a new mechanism for limiting the environmental mobility of contaminants in water by synthesizing calcite crystals and encouraging either incorporation into calcite or co-precipitation of different carbonates, thus converting an

aqueous species into a solid. Carbonates are found in vastly different geologic environments, therefore they are geochemically important and used in contamination studies (Reeder 1983a). Calcite contaminant interaction has a control over the environmental fate of contaminants, with the potential to limit the mobility of several toxic metals (Zachara et al., 1991; Warren et al., 2001; Hay et al., 2002; Kelly et al., 2006; Lashtanove & Stipp, 2007; Heberling et al., 2008). In environmental water, ion-surface interaction can determine the geochemical fate of both the sorbate solution and the sorbent mineral (Hay et al., 2002), contaminants that do not interact with the surface of a specific sorbent (in this case calcite) can have much longer aqueous residence times than those that do.

The trace metals used in this study vary widely in their level of hazardousness. Some trace metals are simultaneously toxic in large quantities and essential micronutrients, like selenium, manganese and cobalt; while others are toxic at all concentration and the desirable concentration in drinking water is set at zero like in lead and arsenic. The contaminants used in this study are all naturally available and reducing the concentration of these contaminants to zero in all drinking water would be too costly. Legal or suggested regulatory limits and maximum contaminant levels are set to reduce the risk of adverse health effects while retaining an economically sensible price for water, and some guidelines are only set for aesthetic reasons (taste, odor or color). Table 2 summarizes the contamination thresholds set for the trace metals of interest in drinking water. Three different guidelines or trace metals were studied whenever possible, The World Health Organization "Guidelines for Drinking-water Quality" [WHO GV]. The United States Environmental Protection Agency "List of Contaminants & their Maximum Contaminant Level" [LoC MCLs] and "National Secondary Drinking Water Regulations"

[NSDWRs] and the West Virginia Department of Environmental Protection “Requirements Governing Drinking Water Standards” [WVDEP]. For some contaminants the different guideless set the same limits, most noticeable the Arsenic guidelines are set at 10ppb in all three systems. The WVDEP was the only agency that set maximum enforceable levels of manganese, which is a secondary standard and is set at 50ppb by the EPA but at 1ppm by the WVDEP.

Element	WHO ¹	EPA ^{2,3}	WVDEP ⁴
Co	N/A	N/A	N/A
Mn	400ppb	50ppb ³	1ppm
Pb	10ppb	15ppb ²	15ppb
Hg	6ppb	2ppb ²	2ppb
As	10ppb	10ppb ²	10ppb
Se	10ppb	50ppb ²	50ppb

Table 2: Drinking water limits for the trace metals of interest. 1. World Health organization “Guideline for Drinking-water Quality”. 2. US EPA “List of contaminants and their Maximum contaminant Level”. 3. US EPA “National Secondary Drinking Water Regulations”. 4. West Virginia Department of Environmental protection “Requirements Governing Drinking Water Standards”.

Cobalt did not have a published guideline level in any of the studies, however the EPA included it to the Contaminant Candidate List 3 in 2009, and again the proposed contaminant list for monitoring under the unregulated contaminant monitoring regulation program (EPA, 2011). The most common industrial application of cobalt includes the production of metal alloys for aircraft engines, magnets, and cutting tools, components in medical prosthetics, and as a pigment in ceramics and paints. Cobalt is classified by the

United States Agency for Toxic Substances and Disease Registry (ATSDR) as a “reasonably anticipated human carcinogen” and exposures to high levels of cobalt can result in lung and heart effects as well as dermatitis. Cobalt is also an essential micronutrient and is a base component of vitamin B12 (ATSDR, 2011).

Like cobalt, manganese and selenium are both essential micronutrients, but in large quantities can cause negative health effects. The consumption of selenium is a double edge sword, because it is necessary for proper function but it can also cause acute toxicity. It has one of the narrowest ranges between dietary deficiency (below 40 µg/day) and toxic level (above 400µg/day) (Aurelio et al., 2010).

Arsenic, lead, and mercury are all highly toxic elements, with known effects to human health and no known nutritional benefits. All three elements are known to cause nervous system damage. Mercury and lead have particularly negative effects when young children are exposed because they cause developmental complications during organ and tissue growth. Mercury is found in 714 of the 1684 National Priorities Lists sites, part of the superfund program, of the EPA, while lead is found in 1272, and arsenic is found in 1149 of the sites. High concentrations of arsenic are also found in some rocks and ground waters across the world, most noticeably Bangladesh, India, Argentina, and Northeast United States (Nordstrom, 2004), and it is considered one of the world most severe cases of inorganic contamination of drinking water (Sø et al., 2008).

Importance of a New Decontamination Method

A water decontamination protocol that can be implemented in remote areas at a low cost will have vastly greater utility than an equally effective protocol that is too expensive or whose implementation requires technical expertise, particularly in developing nations. We

have the current technology to decontaminate many places that experience with high levels of toxic metal pollution, like some waterways near metal finishing and metallurgical sectors. Many of the current process, however, require large investment in infrastructure and labor, and often create sludge disposal problems, when the contaminants are gathered in a condensed liquid form that needs to be isolated from traditional waterways (García-Sánchez and Álvarez-Ayuso, 2002).

An effective decontamination protocol needs to be able to lower the contamination below the safe limit, while keeping the costs low and the methodology simple. Several studies have proven that sorption is an effective metal removal system (Zachara et al., 1989; Lorens, 1981, Davis et al., 1987); however, sorption can be a temporary solution (Sø et al., 2008). It is necessary to have a method that can maximize incorporation of contaminants into the crystal and not just at the surface and this is more likely if the crystal grows in the presence of contaminants. Due to the step growth nature of calcite crystallization, elements with proven high sorption rates should be able to react with the surface of the crystal and then be more permanently incorporated as the crystal grows around it.

The synthesis procedure for a decontamination process would create crystals that are large enough for maximizing total incorporation and facilitating removal of the solids from the aqueous solutions need to be large enough to easily filter, and grow slowly enough to incorporate crystals through both substitution into lattice sites and sorption into the surface of inner crystal layers. Several methods currently exist to synthesize calcite crystals, some even provide high-quality crystals of the appropriate size; these approaches are more complex and challenging than ideal for working with metal hazards. The method

used throughout these experiments uses low cost approach and a simple one step synthesis to creates sub-millimeter sized crystals that are easy to filter out of water leading to a low costs separation of solids and liquids.

Other synthesis methods do not have the necessary combination of simplicity, high yield, and low cost necessary for an adequate universally deployable decontamination application. Some methods are inappropriately complicated for field application, using very specialized laboratory apparatus like a high gravity precipitation system or a rotating package bed with multiple gas inputs (Agnihotri et al., 1999; Gao et al., 2007; Chen et al., 2000; Gupta and Fan, 2002; Sun et al., 2011; Isopescu et al., 2011). Some methods include very complicated organic inputs, which are expensive and not readily available to the general public (Wakita et al, 1985; Hirai et al., 1997; Xu et al., 1998; Faatz et al., 2004; Guo et al., 2011), and most methods produced nano sized calcite crystals that are not as easily filtered out of the solutions (Naka and Chujo, 2001; Donners et al, 2002; Liu et al., 2011; Cai et al. 2010).

Materials and Methods

Calcite Synthesis

Calcite crystals were synthesized in acidified water doped with trace metals at different concentrations based on a novel synthesis procedure. This approach is a modification of a simple inorganic aqueous synthesis for sparingly soluble salts (Fernelius and Delting, 1934). The original approach involved a larger setting and was not successful for growing micro-sized crystalline calcite. A change in the pH of the initial solution to between 2.05-2.20 by adding 1 M HCl, however, resulted in euhedral calcite crystals (Morrison et al., forthcoming). The method presented here is a further modification from Morrison et al. adapted to lower the costs of the final product with the goal of increasing its applicability in decontamination work.

The experimental apparatus consisted of a 150mL Pyrex beaker containing two small scintillation vials (approximately 3mL, 2.5cm tall) (Figure 3). Saturated solutions of CaCl_2 and $(\text{NH}_4)_2\text{CO}_3$ were prepared by adding 0.36 g of CaCl_2 (ACS grade; AMRESCO) and 0.50 g of $(\text{NH}_4)_2\text{CO}_3$ (ACS grade, Alfa Aesar) to 2mL of ultrapure H_2O . The two small vials were placed at either side of the beaker, not in contact with the beaker wall or each other. The saturated solutions were placed in each vial, so that 2mL of the CaCl_2 solution were in one vial and 2mL of the $(\text{NH}_4)_2\text{CO}_3$ solution were placed in the other. Both vials were slowly filled completely with the desired acidified solution, so that the pH of the filler solution was between 2.05-2.20. Different amounts of 1M HCl were used to acidify the solutions. The initial concentrations of trace metals in the filler solutions as well as the initial pH of the 115 mL of acidified solution were added carefully to the beaker, without disturbing the small vials already in place as seen in Table 3.

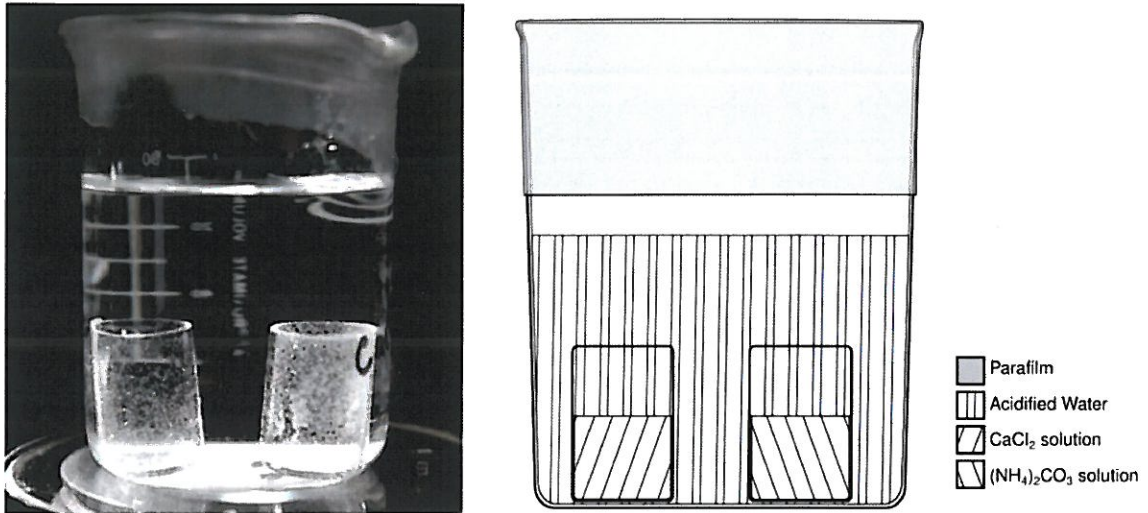


Figure 3: (Left) Picture of the actual experimental apparatus. (Right) Schematics of the system indicating the locations of individual components.

Trace Metal Addition

Experiments with three blanks as well as three repetitions of every concentration of trace metals were set up (Table 3). Each metal had at least three different concentrations - “low”, “medium” and “high” - and a fourth concentration for Hg^{2+} - with an extra “very low” concentration. The low concentration for As^{3+} , Se^{4+} , Pb^{2+} as well as the lowest concentration for Hg^{2+} were set at the EPA List of Contaminant’s Maximum Contaminant Level. The low concentration for Mn^{2+} was set according to the EPA’s National Secondary Drinking Water Regulations (secondary standards). The level for Co was set at 100ppb, since the EPA did not have a drinking water regulation level. The low concentration of Hg^{2+} was 10 times the “very low” value. The medium concentrations were set at 10 times the low concentrations and the high concentration was set at 1000 times the maximum contaminant level.

Experiment #			Trace Metal	Concentration	pH
1a	1b	1c	Blank	0	2.15
2a	2b	2c	Co ²⁺	100ppb	2.15
3a	3b	3c	Co ²⁺	1000ppb	2.19
4a	4b	4c	Co ²⁺	10 000ppb	2.12
5a	5b	5c	Mn ²⁺	50ppb	2.18
6a	6b	6c	Mn ²⁺	500ppb	2.14
7a	7b	7c	Mn ²⁺	50000ppb	2.08
8a	8b	8c	Pb ²⁺	15ppb	2.11
9a	9b	9c	Pb ²⁺	150ppb	2.11
10a	10b	10c	Pb ²⁺	15000ppb	2.15
11a	11b	11c	Hg ²⁺	2ppb	2.13
12a	12b	12c	Hg ²⁺	20ppb	2.14
13a	13b	13c	Hg ²⁺	200ppb	2.13
14a	14b	14c	Hg ²⁺	20000ppb	2.14
15a	15b	15c	As ³⁺	10ppb	2.13
16a	16b	16c	As ³⁺	100ppb	2.10
17a	17b	17c	As ³⁺	10000ppb	2.20
18a	18b	18c	Se ⁴⁺	50ppb	2.12
19a	19b	19c	Se ⁴⁺	500ppb	2.06
20a	20b	20c	Se ⁴⁺	50000ppb	2.15

Table 3: Samples and initial solution conditions.

The study contained a total of 60 experiments. A sample of 30mL the solution used in each experiment was taken before the experiments were set up, day 0, then another sample was taken on day 10. For every contamination level (one of every 3 experiments) one sample was also taken at day 5. After the 10th day, the solids were removed and placed in small Petri dishes. The solid samples were viewed under a petrographic microscope

under both plane polarized and cross polarized light. The dominant crystal morphologies in each solid sample were identified and pictures were taken.

X-Ray Diffraction Analysis

Based on the results from the optical analysis, a limited number of solid samples, representing the major morphologies, were powdered and analyzed using Washington and Lee University's X-ray Diffractometer. The list of solid samples analyzed using the XRD can be seen in Table 4. Individual scans were corrected for background using image processing software and then compared to high quality standard spectra of different minerals. Most of the standards were obtained from the RRUFF project database (2006). Additionally other mineral standards collected from RRUFF were used - Sphero-cobaltite (R050497), Barytocalcite(R050288), Aragonite(R040078) and Cerussite(R040069) standards. The vaterite standard used was based on a synthetic samples spectrum in Kamhi (1963).

Sample #	Sample Characteristics	Sample #	Sample Characteristics
1c	Blank	2a	Co 100ppb (Co low)
15a	As 10 ppb (As low)	3a	Co 1000pp (Co med)
16a	As 100ppb (As med)	4b	Co 100000ppb (Co high)
18a	As 10000ppb (As high)	4c	Co spheres
10a	Pb 15000ppb (Pb high)	4d	Co prism

Table 4: List of solid samples analyzed with X-ray Diffraction.

Inductive Coupled Plasma Optical Emission Spectroscopy

ICP-OES data was collected at Washington and Lee University with a Spectro Ciros ICP-OES. The liquid samples taken on day 0, 5, and 10 for Co^{2+} , Mn^{2+} , As^{3+} , Pb^{2+} , Se^{4+} as well as the final solid and the blank samples were analyzed using different concentration standard solutions made with QCS-27 (high purity standards). The samples were grouped according to the concentrations of trace metals in the initial liquid (low, medium, high) to create a set of standards within one or two orders of magnitude. The count rate was

converted to ppb using a second-order polynomial regression. The detection limit was calculated using Equation 2, from Skogerboe and Grant (1970) at 0.95 and 0.99 confidence level.

$$DL = \frac{SD_{blank} t_{(n-1,CL)}}{da/dc}$$

Equation 2: Skogerboe and Grant (1970) Detection Limit. SD is the standard deviation of count rates for n blanks. t is the student statistic at a specific confidence limit. da/dc is the slope that describes the relationship between the count rate and the known concentrations for the standards at various dilutions (ppb).

The estimate percentage error for each sample was determined by computing a power regression between the calculated percentage error for all of the standard concentrations and the concentration. This follows the analytical observation that the percentage error for very small quantities is larger than the percentage error for larger quantities.

Mercury and the ICP-OES. In order to optimize the levels of mercury preservation in aqueous solutions all the Hg^{2+} samples were treated with 1ppm $AuCl_3$. This was based on the success of EDRB-LV researchers in stabilizing aqueous mercury with 1ppm $AuCl_3$ and 2% HNO_3 (US EPA, 2003), all mercury samples were analyzed in a separate analytical run.

Ion Chromatography

The Dionex ICS-2100 Ion Chromatograph (IC) at Washington and Lee University was used to analyzed for six key cations (Na^+ , K^+ , NH_4^+ , Ca^{2+} , Mg^{2+} , Li^{2+}) in day 5 and day 10 samples as well as the $CaCl_2$ and $(NH_4)_2CO_3$ solutions used in the calcite synthesis, each sample was analyzed for 15 minutes. The resulting peak areas were analyzed using a

combination of Dionex software (Chromeleon) and image processing software. The different peak areas were calibrated by computing linear and second-order polynomial regressions based on the peak areas of known standards at different levels of dilution. The detection limits were calculated using equation 2.

ICP-Mechanical Separation

In an effort to reduce the cost of the final apparatus this study used ACS grade reagents (95% pure CaCl_2). It was necessary to treat the original CaCl_2 and $(\text{NH}_4)_2\text{CO}_3$ solutions to increase their purity. In order to maximize the output of larger crystals a study was conducted to test the effectiveness of different combinations of centrifuging and double filtering the samples (with a $0.45\mu\text{m}$ and then a $0.20\mu\text{m}$ Fisher filters).

Four different mechanical separation methods to purify the saturated CaCl_2 and $(\text{NH}_4)_2\text{CO}_3$ solutions were tested. Method 1 consisted of centrifuging the solution then removing suspension and leaving behind the brown residue (still in liquid form). Method 2 simply involved double filtering the solution (at $0.45\mu\text{m}$ and then $0.20\mu\text{m}$). Method 3 entailed centrifuging the solution and then double-filtering the suspension. Finally, Method 4 required double filtering the solution then centrifuging the remaining liquid and removing only the top most part of the liquid. The resulting clearer solutions of saturated CaCl_2 and $(\text{NH}_4)_2\text{CO}_3$ were analyzed using the ICP-OES Spectroscopy at Washington and Lee University (Figure 4).

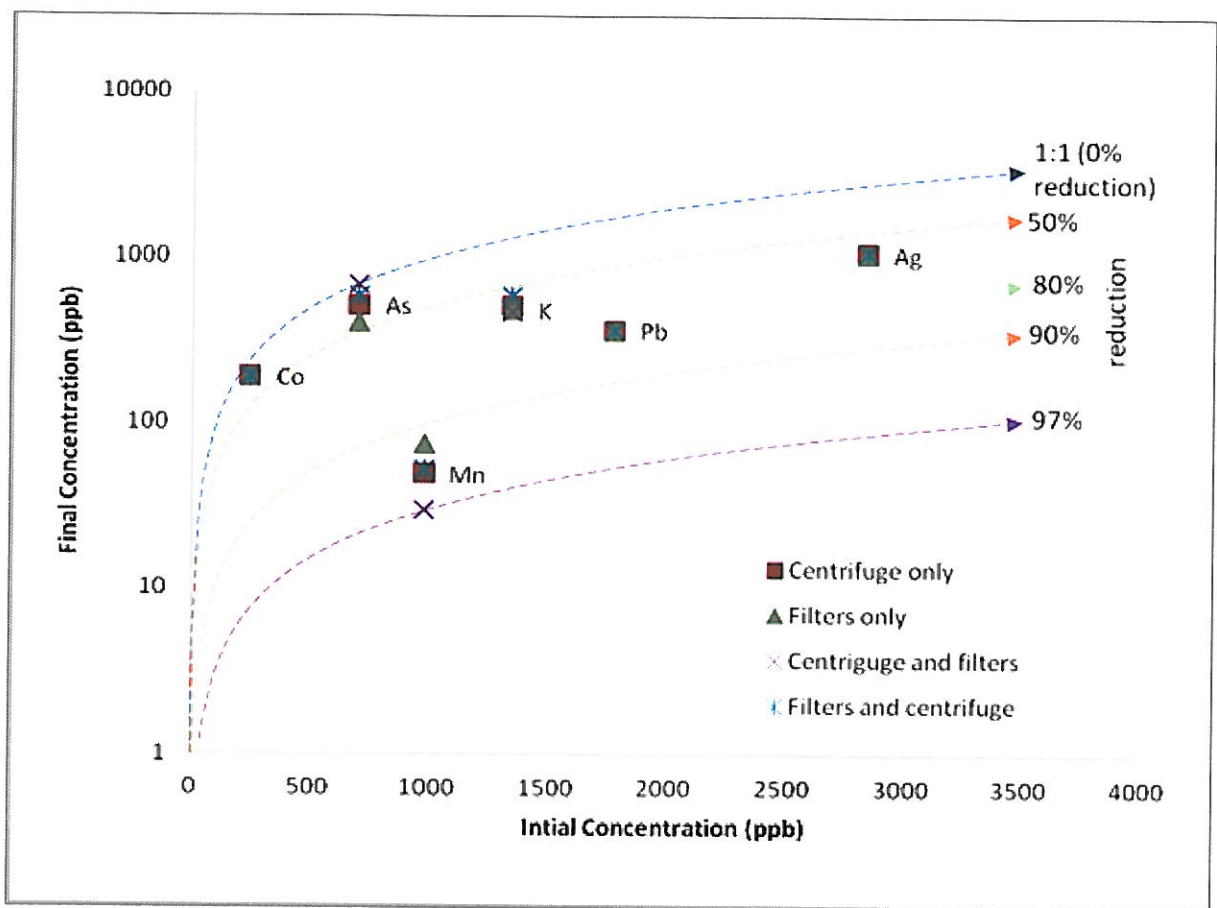


Figure 4: Mechanical separation results. The different dotted lines indicates the percentage reduction in an element between the untreated concentration and the treated concentration.

For the most part, every method is equally efficient in reducing the levels of contaminants in the resulting liquid. The levels of cobalt were not highly affected by any of the method. Arsenic was reduced most effectively through method 2. Manganese was highly reduced in all methods, but slightly most effectively in method 3. Silver, potassium and lead were all similarly reduced by the four methods.

The double filtering method used in Method 2 was selected as the ideal purification method because of it reduced the levels of all elements and it was the most effective in reducing arsenic level. The CaCl_2 and $(\text{NH}_4)_2\text{CO}_3$ solutions for all the final experiments were double filtered before being placed in the vials.

Results

Solid samples were analyzed optically to determine the dominant morphologies, then a representative group of samples was powdered and analyzed by X-ray Diffraction to determine the dominant crystal structures. Every sample was then dissolved in acid and the liquids were analyzed using ICP-OES and IC to determine the concentration of key elements. The following section presents the results from each analytical technique.

Optical Analysis

The solid samples consisted of sub-milimeter sized crystals, mostly ranging from 50 μm to 500 μm . The crystals were mostly colorless to light yellow, with the exception of the high concentration cobalt samples which had some pink to light purple crystals. The dominant morphology across all of the experiments was euhedral calcite rhombohedral crystals, most crystals exhibited perfect cleavage in three directions (Figure 5); Most samples were dominated by relatively large, euhedral calcite crystals (Figure 6); however, conglomerations of cryptocrystalline material were also commonly present (Fig 6, top right corner). The cryptocrystalline material was originally believed to be amorphous powder; however, the powder exhibited low birefringence when looked under cross polarized light which indicated that it was not amorphous but crystalline (Figure 7).

Two different contaminants showed distinct morphologies that were not readily identified as calcite crystals. The high concentration manganese experiments (Figure 8) showed distorted rhombohedral crystals, tabular conglomerations and platy cryptocrystalline assemblages that were not morphologically similar to calcite. The manganese samples were colorless to light brown. Some manganese doped crystals also

exhibit anomalous interference colors, a brown coating visible both under plane polarized light and cross polarized light.

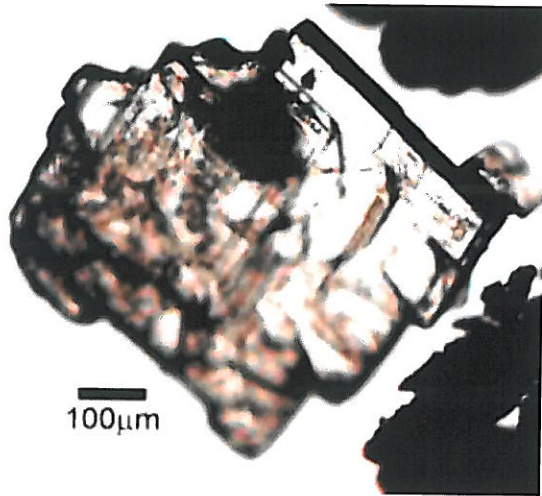


Figure 5: A euhedral calcite crystals. Experiment 11a (2ppb Mercury). Magnification: 40 x. Plane polarized light.



Figure 6: Experiment 1a (blank) at 40x magnification and plane polarized light.

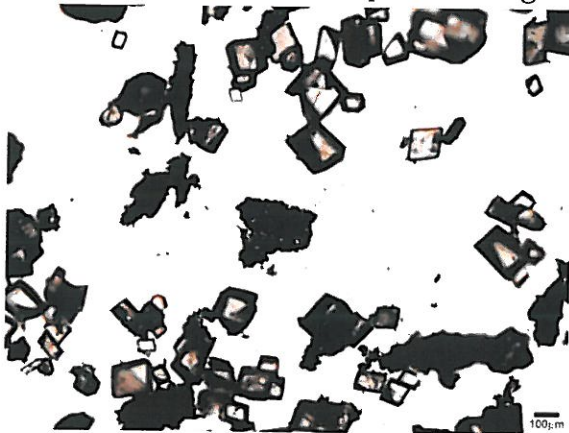
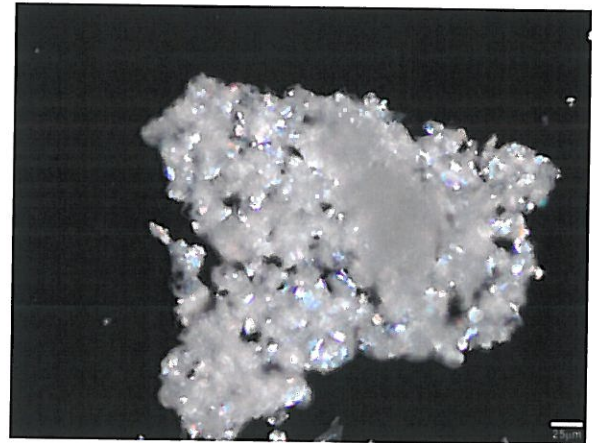


Figure 7: (left) Experiment 2b, cobalt 100ppb, at 40x under plan polarized light. (right) Experiment 2b at 200x under cross polarized light.



The highest concentration of cobalt experiments, 100ppm cobalt, also showed some non-euhedral shapes. The dominant crystal color was pink to light purple, and very few crystals were colorless. Additionally, the crystals did not manifest traditional calcite morphologies. The dominant crystals were elongated prism and small crystal

conglomerations in the form of spheres (Figure 9). The crystals also showed anomalous interference colors. The spherical crystals were initially thought to be the cobalt carbonate equivalent of calcite –spherocobaltite, the end member of the calcium carbonate to cobalt carbonate solid solution. This explanation seemed unlikely after examining the X-ray diffraction results because spherocobaltite, if present, would be a minor component of the samples (see Results, X-ray diffraction).

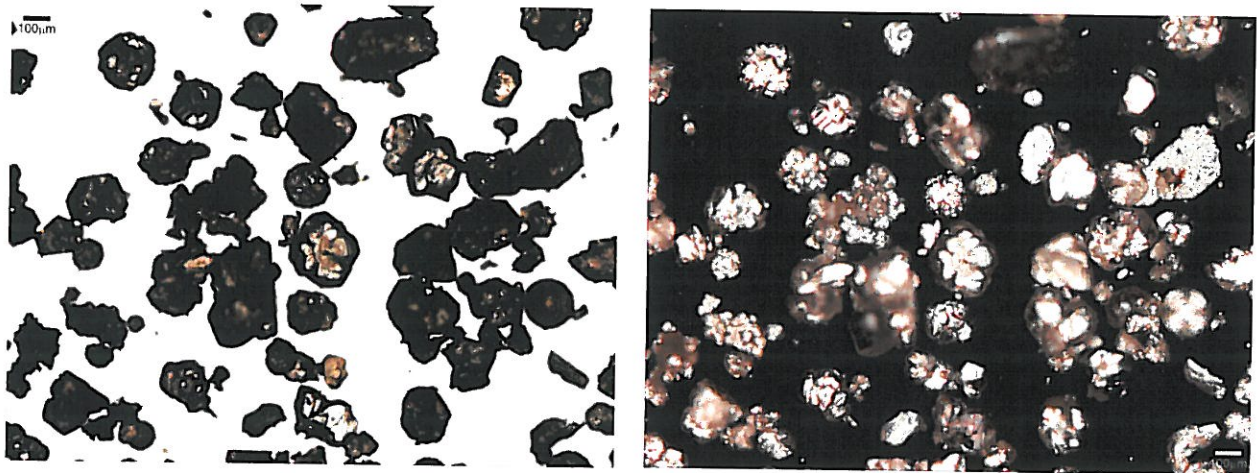


Figure 8: Experiment 6b, 50ppm manganese. Left: under plane polarized light, 40x magnification. Right: cross polarized light, 40x.

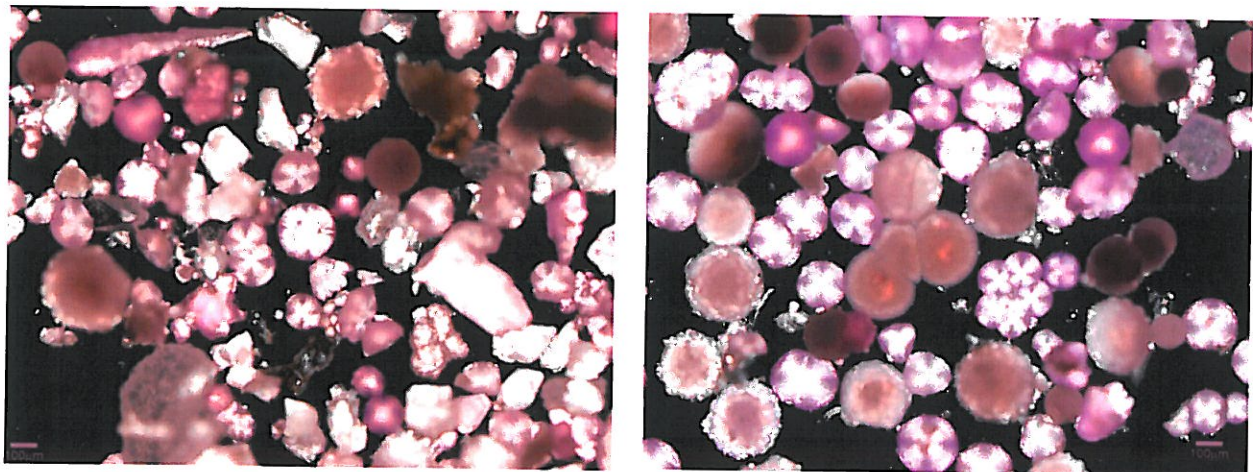


Figure 9: Experiment 4b, 100ppm cobalt. Left: cross-polarized light, 40x. Right: just spheres, cross-polarized light, 40x.

X-ray Diffraction

Based on the results of the optical analysis, a sub-set of solids were selected for an X-ray diffraction analysis (Table 4). The resulting XRD spectra show that calcite was the major mineral present in all of the samples (Figure 10). All of the sample ran had strong calcite peaks and those morphologically similar to calcite, arsenic, lead, blank and low concentrations of cobalt show a standard calcite spectrum with some minor peaks that correspond to the vaterite spectrum (in red).

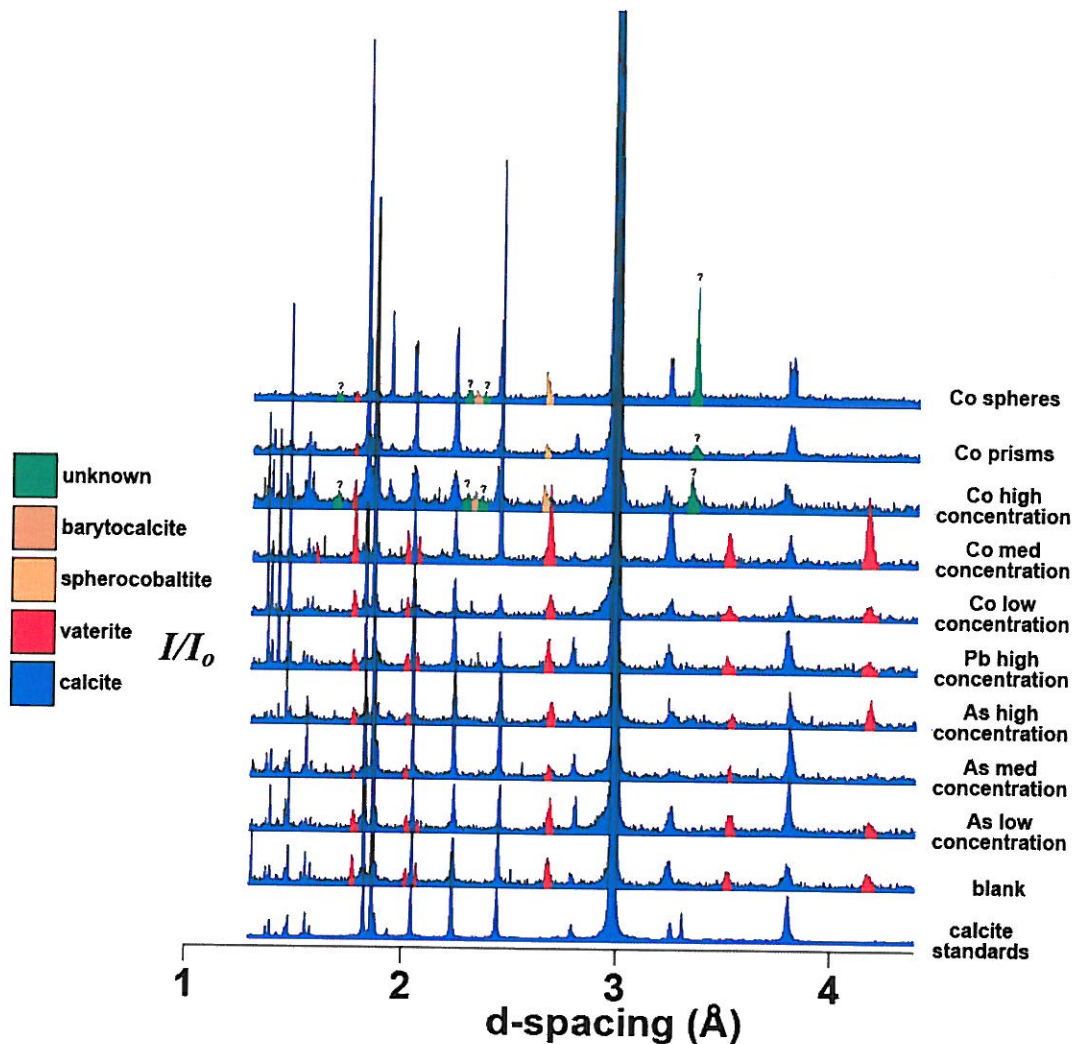


Figure 10: X-ray diffraction spectra, all samples are background corrected and intensity corrected. I_0 is the maximum peak height. The maximum value of I/I_0 is 100.

The morphologically distinct samples that were analyzed -high concentration of cobalt, cobalt prisms and cobalt spheres, also display a strong calcite signal; however, vaterite had a smaller presence. The high cobalt, cobalt spheres, and cobalt prisms spectra all had a minor peak that was located at the position of the highest intensity peak for spherocobaltite. Unfortunately, both the vaterite and the spherocobaltite maximum intensity peaks are located in the same region $\sim 2.75 \text{ \AA}$. The peak overlap thwarts the definite identification of the minor mineral components of the sample.

ICP – Trace Metals

The liquid concentrations of every trace metal were plotted against time -day 0, day 5 or day 10 of the experiments. For access to the full data contact the Washington and Lee Geology Department (geology.wlu.edu). The difference between the initial trace metal concentration, at day 0, and the final concentrations, at day 10, can be seen in the distance the y-axis. The initial levels of cobalt in the liquid were reduced through the experiment for all concentration of cobalt (Fig 11). All of the cobalt experiments in this study experienced rates of contaminant reduction above 90 percent. The medium concentration had the lowest final/initial ratio, while the low and the high concentration experiments had similar rates. The background level of cobalt is above the detection limit for the low and the medium concentration runs, while it was below detection on the highest concentration experiments.

The manganese doped experiments resulted in similar outcomes to the cobalt experiments (Figure 12). The final concentrations of manganese were also highly reduced compared to the initial concentrations, with the day 10 concentrations below the detection limit for all the concentrations. The initial and the medium concentration experiments

transitioned between being above the EPA's National Secondary Drinking Water Standards to being below them. The medium concentration also varied from above the World Health Organization guideline, 400ppb, to below it. The high concentration experiments was also reduced to levels right below the West Virginia Department of Environmental Protection "Requirements Governing Water Quality Standard".

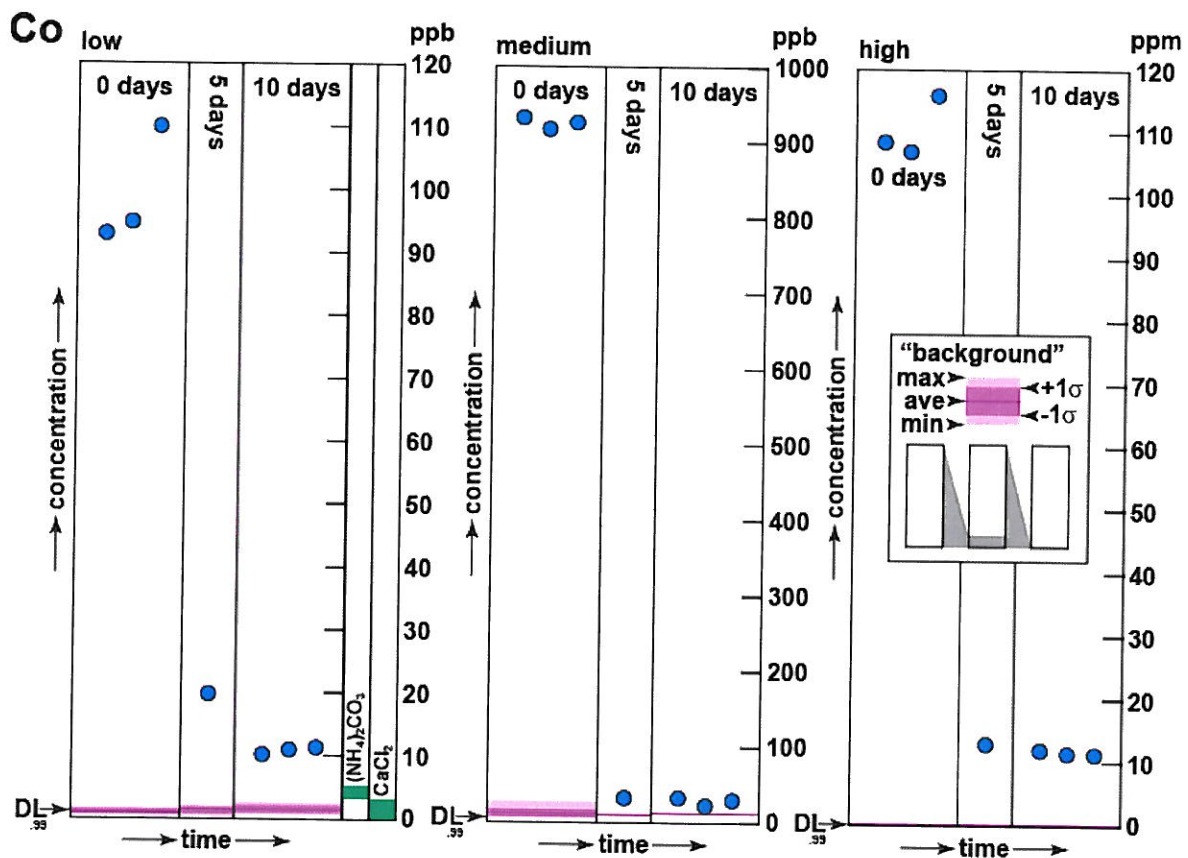


Figure 11: ICP-OES results for cobalt. Experiments 2a-4c. The background lines are based on the measured levels of cobalt for non-cobalt doped samples. The detection limits are shown in the lower left corner of each graph. The green bars next to the low concentration cobalt shows the measured amount of cobalt present in the samples according to the ICP – mechanical separation analysis.

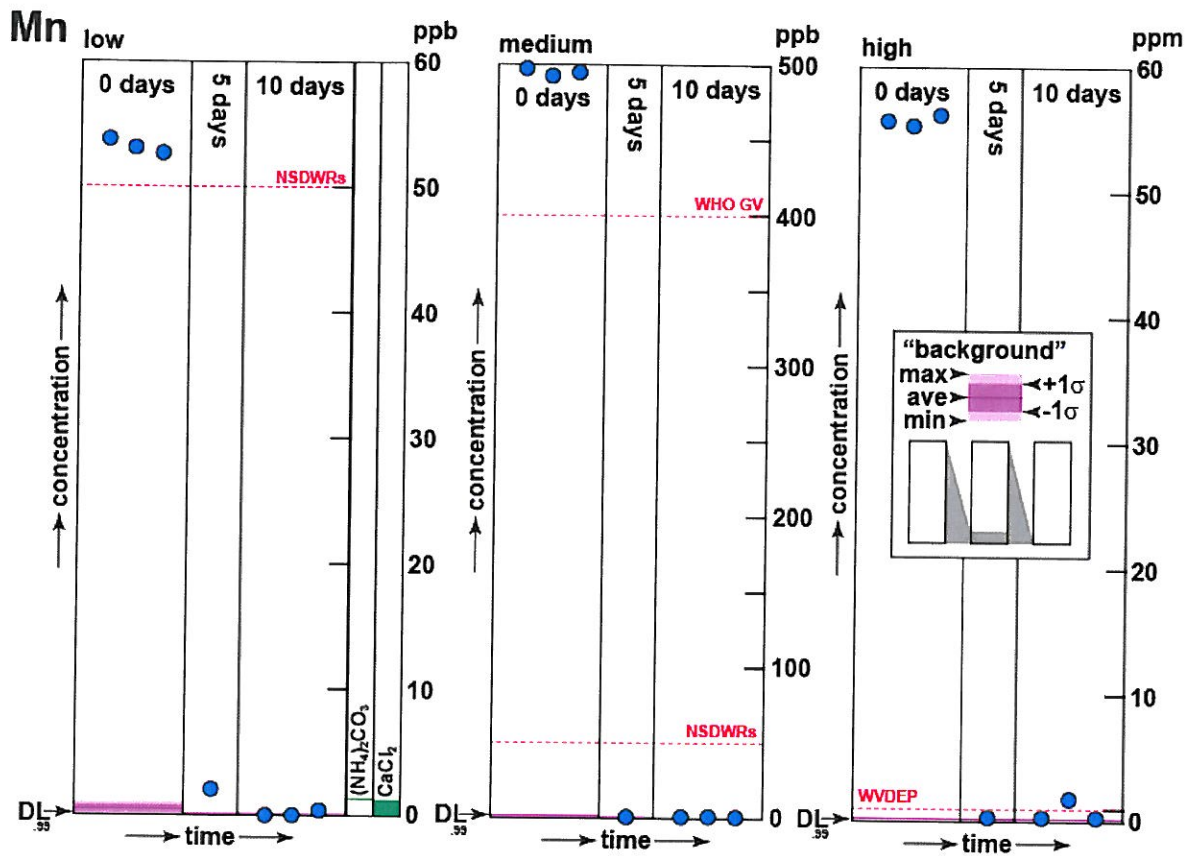


Figure 12: Manganese ICP-OES results. Experiments 5a – 7c. The dotted red lines indicate the EPA's NSDWRs, the WHO guideline and the WVDEP limit. Symbols are the same as in Figure 11.

The lead experiments had a much more limited reduction in trace metal concentrations at the low and medium concentration level, but significant reduction at the high concentration levels (Figure 13). The background levels of lead were substantial at the low and medium concentrations. At the low concentration, the detection limit was below the highest background signal, and all the final concentration levels were below the detection limit. The detection limit was also above the WHO drinking water guideline for lead; however, it was below the EPA level. At the low concentrations, the final lead value was below the EPA limit. The background level rose throughout the experiment from below detection on day 0 to above detection limit and just below the EPA Maximum Contaminant

limit. For the medium concentration the final values also overlapped with the final level of background in non-lead experiments.

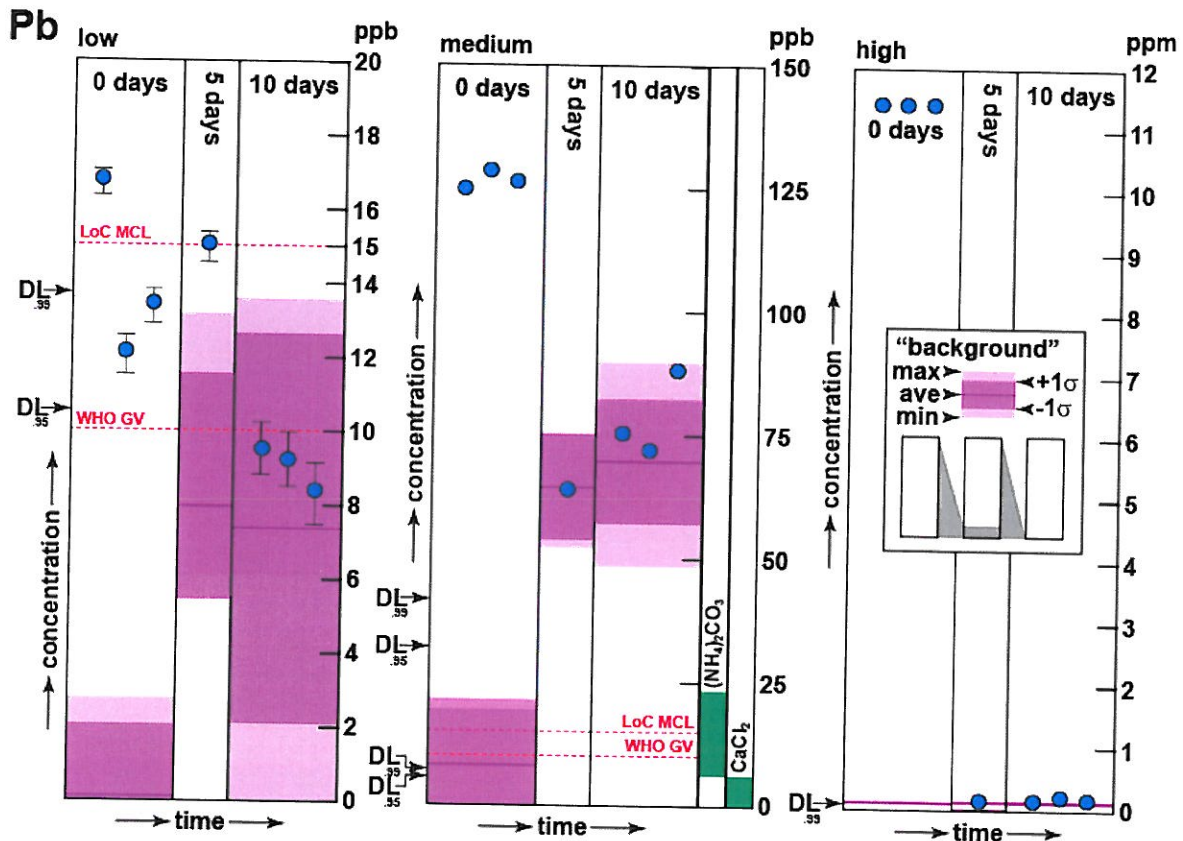


Figure 13: Lead ICP-OES results. Experiments 8a-10c. Symbols are the same as in Figure 11.

The levels of arsenic also increased throughout the low and the medium concentration experiments, but remain relatively stable at the highest concentration (Figure 14). The final values of arsenic for the low concentration experiments are highly variable, and range from remaining relatively stable to increasing considerably. The background amounts of arsenic increased continuously from day 0 to day 10 which suggests that the other experiments were becoming enriched in arsenic.

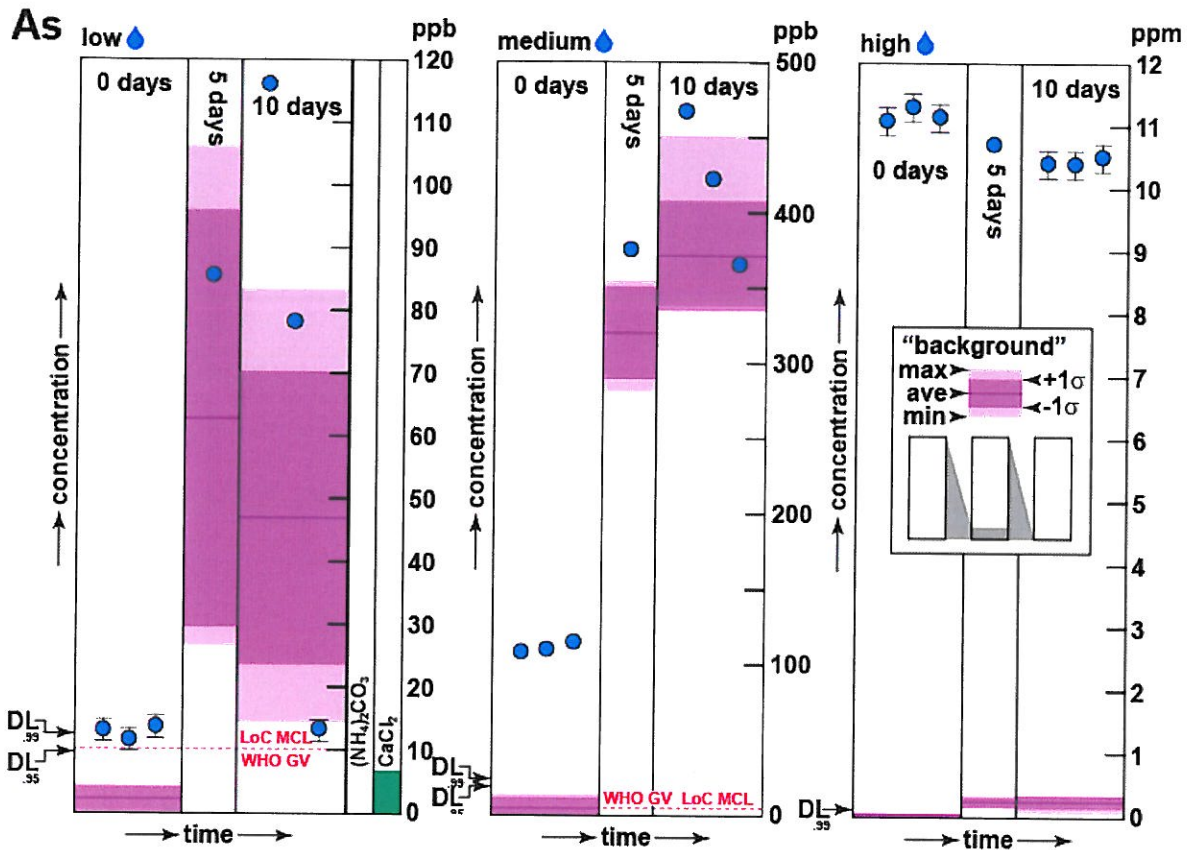


Figure 14: Arsenic ICP-OES results. Experiments 15a-178c. Symbols are the same as in Figure 11.

The selenium concentrations in the solution were less responsive to the calcite synthesis (Figure 15). There was a slight increase in the selenium concentrations at the low levels. At the medium concentration selenium seemed unresponsive, remaining the same throughout the experiment. At the high concentration, there was a ~60% reduction in the levels of selenium. At the low concentrations, the background level was above the detection limit and at day 10 it encompasses the entire range of the data. At medium levels, the background was only a small fraction of the range and at high levels it became insubstantial.

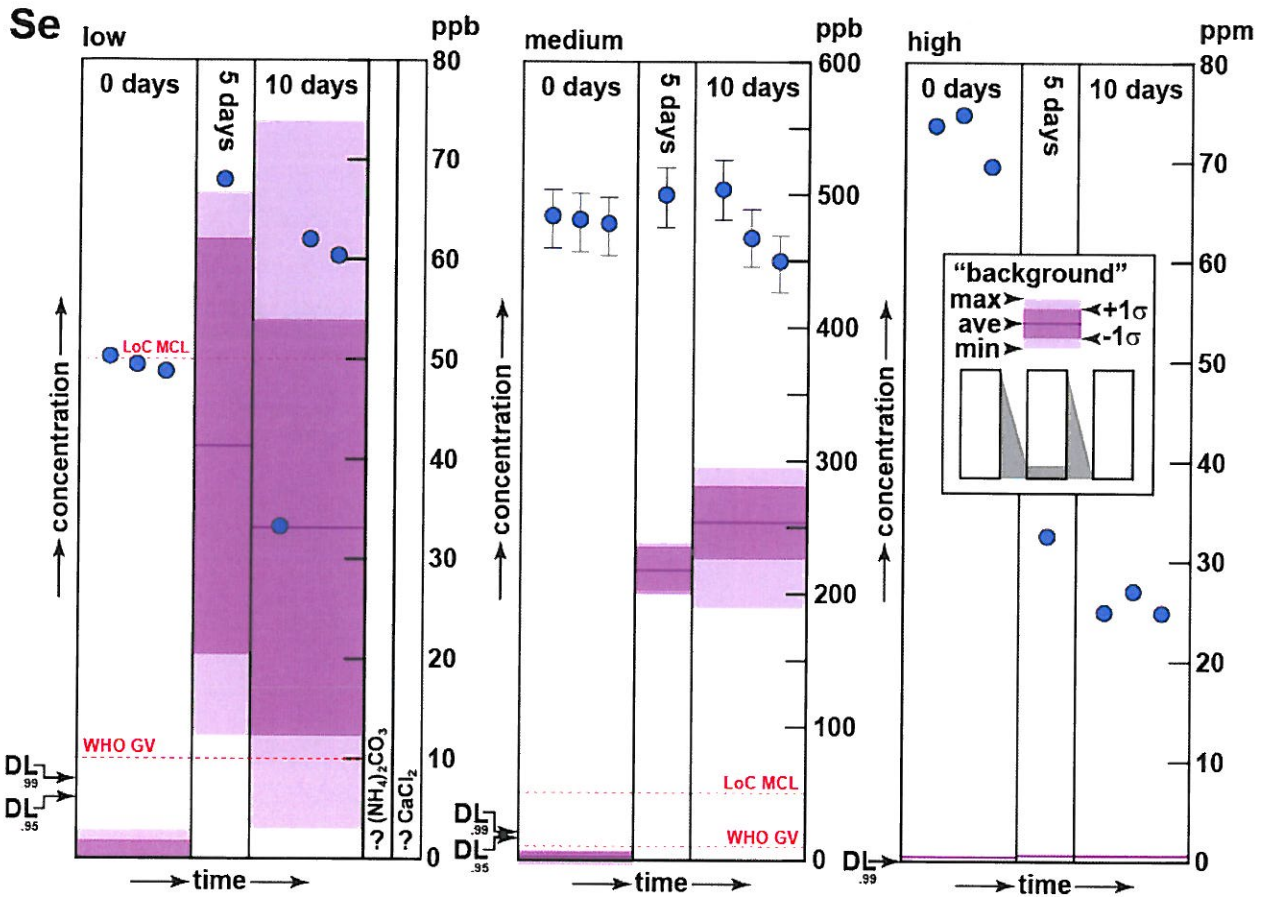


Figure 15: Selenium ICP-OES results. Experiments 18a-20c. Symbols are the same as in Figure 11.

The mercury experiments showed a relative increase in the amount of mercury for the lower concentration experiments but a decrease in the high concentration set (Figure 16). The very low, low, and medium concentration experiments had a very high relative detection limit. Even though the lower concentration experiments began at three different initial concentrations, they had results within the same order of magnitude, with the final concentration at 3ppm. For the high concentration experiments, there was a modest decrease in mercury concentration from initial to the final values. These were substantially above the detection limit.

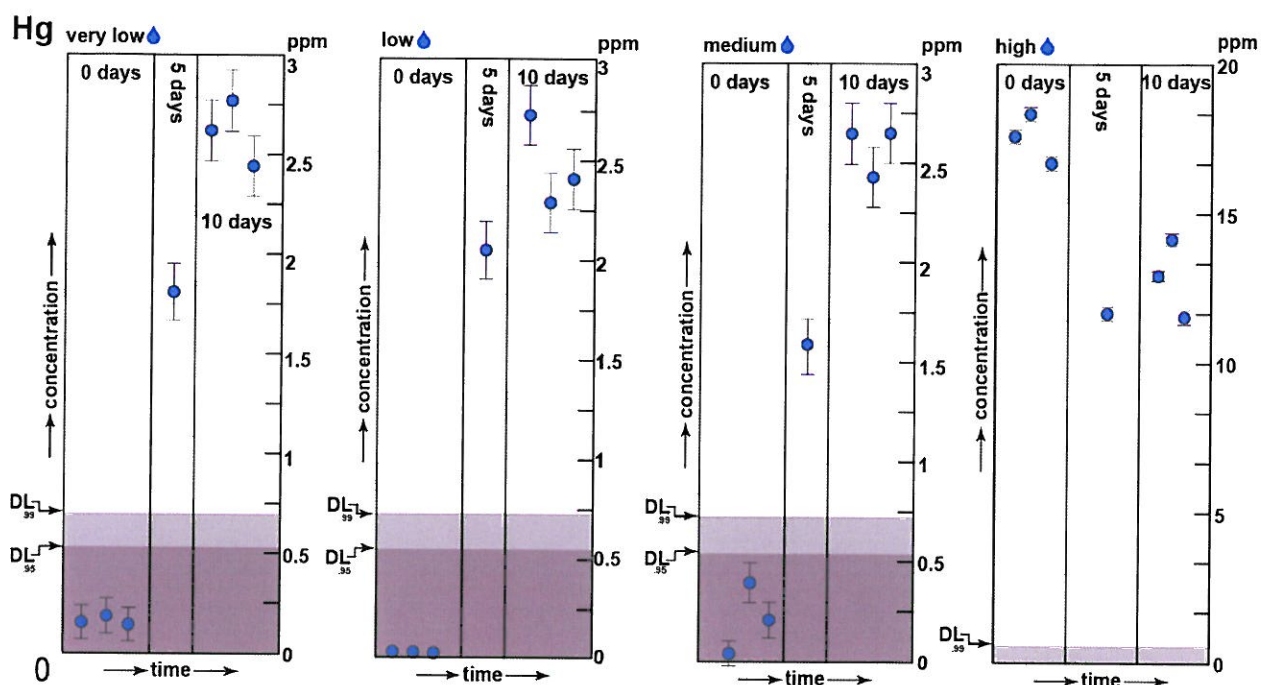


Figure 16: Mercury ICP-OES results. Experiments 11a-14c. Due to the lack of background values from non-Mercury samples, the detection limit region is shadowed in light purple. Symbols are the same as in Figure 11.

Ion Chromatography

The Washington and Lee Ion Chromatograph was used to determine the concentration of major cations in the initial reagent as well as day 5 and day 10 samples. Small amounts of lithium were found in some of the samples but not consistently throughout the experiment. Concentrations of potassium between 190 and 500 parts-per-billion were also present in some samples but not detectable in most samples. Concentrations of sodium on the order of 400 parts-per-billion were present in all samples except for the ammonium initial concentration. The concentration of sodium remained relatively constant throughout the experiment. The initial concentration in CaCl_2 solution was 496 ppb and the average concentration in the final solutions was 621 ppb.

The calcium concentrations in the final liquid samples varied greatly between the initial calcium concentration, at 383parts-per-million, and the day 5 and day 10 concentrations (Figure 17). The day 10 and day 5 concentrations were mostly under 10ppm, with the exception of the low manganese concentration who final concentration was 23ppm. For arsenic, lead, and selenium, the amount of calcium decreases from day 5 concentration to the final liquid concentration. For manganese and cobalt, however, the amount of calcium increased between the middle samples and the final samples. The day 5 samples were lower than the day 0 amounts in all samples, however there was variation in the difference between the day 5 concentration of cations and the day 10 concentrations.

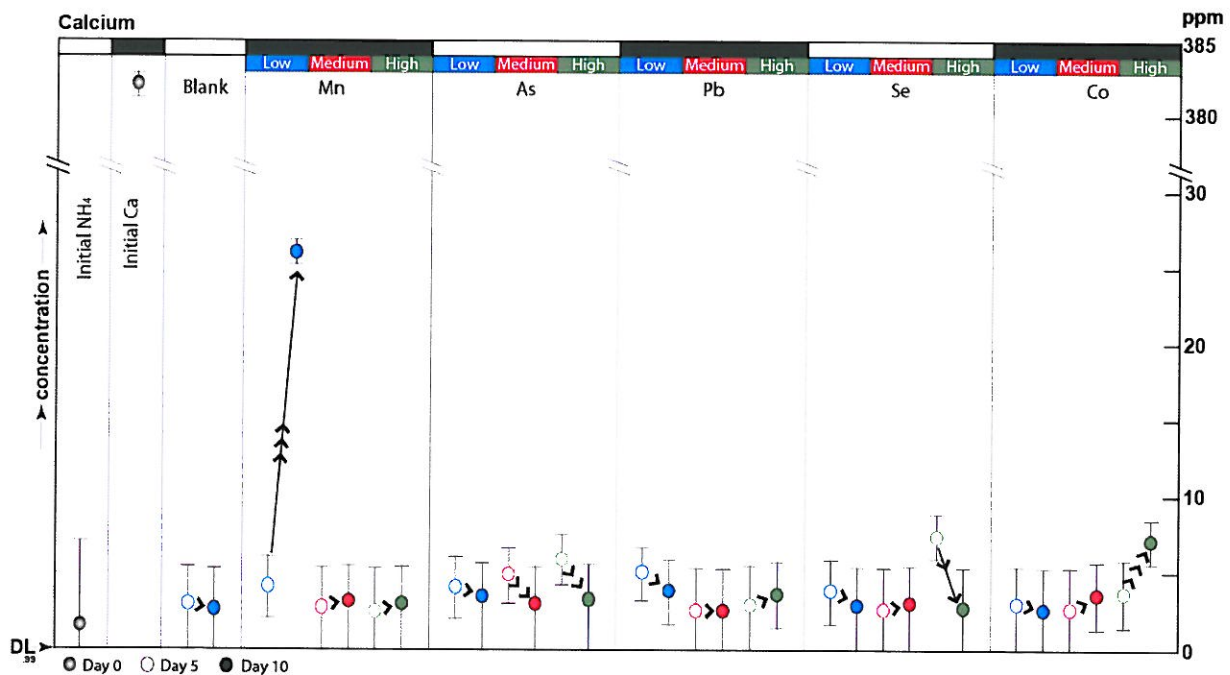


Figure 17: IC results for calcium for Mn, As, Pb, Se, Co doped solutions. The arrows indicate the trend between day 5 and day 10 samples.

All of the final solutions had high concentrations of ammonium, between 450 and 500ppm (Figure 18). The initial concentration of ammonium, 500ppm, is slightly reduced in some of the samples. The day 5 sample had consistently lower concentration of

ammonium that the day 10 samples for the same trace metal and concentration. There was also a decrease in the concentration for magnesium through the experiment (Figure 19). The initial levels of magnesium were provided mostly through by CaCl_2 solution -360 parts-per-billion while the $(\text{NH}_4)_2\text{CO}_3$ had below detection limits concentration of magnesium. The concentration of magnesium in the final solutions had lower level of magnesium ranging from 200 to 300 ppb. Similarly to the ammonium pattern, the day 5 concentrations were below the day 10 concentrations.

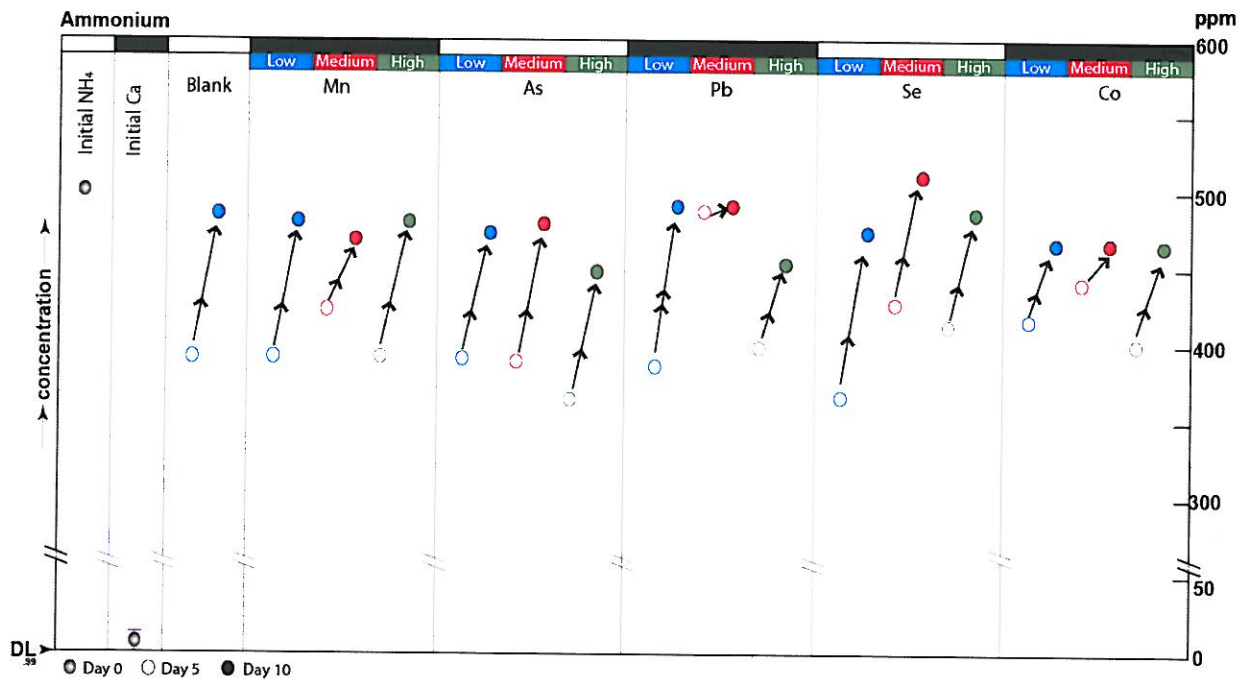


Figure 18: IC results for ammonium for Mn, As, Pb, Se, Co doped solutions. The symbols are the sample as figure 17.

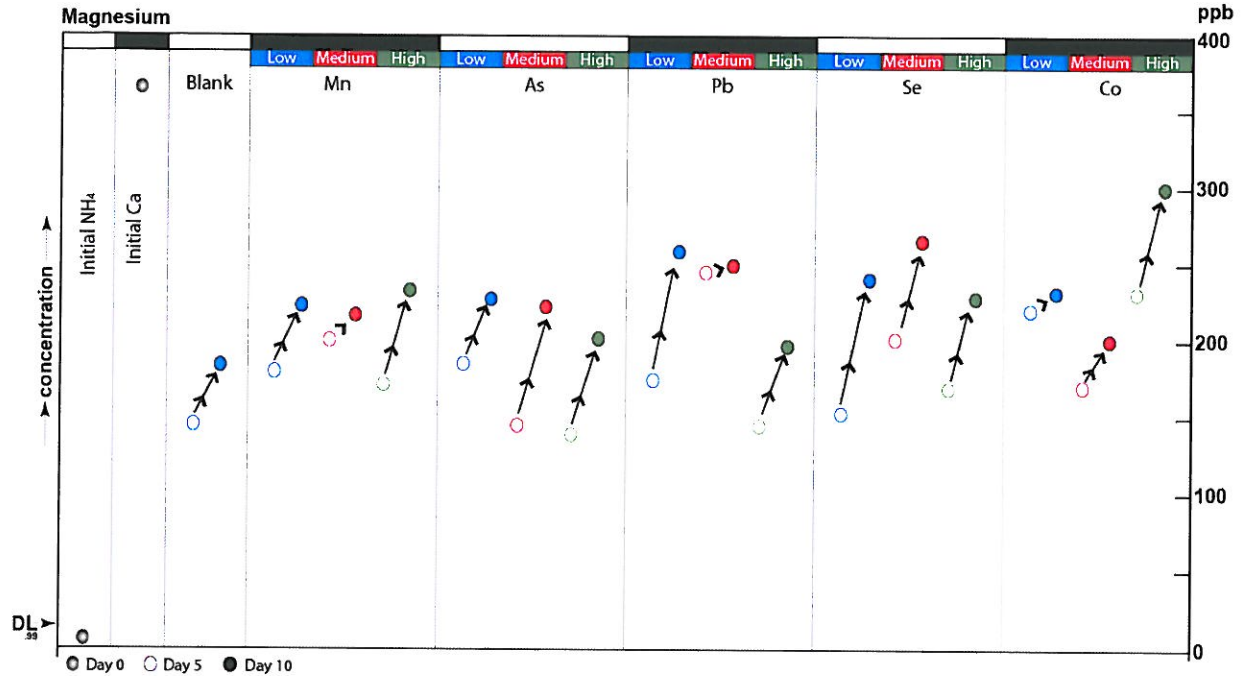


Figure 19: IC results for magnesium for Mn, As, Pb, Co doped solutions. The symbols are the sample as figure 17.

Partition Coefficients

The ICP-OES results for solid samples were used in computing the K_D value for the partition between liquid and crystal (Figure 20). The highest K_D values belonged to the manganese experiments. Selenium at low concentration had the second highest K_D , although this value seems to be an outlier. Lead and cobalt had similar partition coefficient for the range of concentrations, and arsenic had consistently the lowest results.

Table 5 contains the data from the ICP solid crystal run, converted to milligrams of trace metal. The ionic radii are the values as stated by Shannon (1976) for octahedrally coordinated cations based on the speciation originally added to the system. The K_D value was calculated by dividing the total amount of element in the solid by the amount in the liquid.

	ionic radius	Solid (mg)	Final liquid (mg)	Kd
Mn Med	0.83	0.05288	0.00003	1623.01
Mn Low	0.83	0.00755	0.00001	964.74
Se Low	0.64	0.51558	0.00595	86.70
PB High	1.19	1.78721	0.02073	86.20
Co Med	0.75	0.11468	0.00317	36.23
Mn High	0.83	1.26494	0.07513	16.84
Pb Low	1.19	0.01478	0.00104	14.24
Se Med	0.64	0.63426	0.05435	11.67
Co Low	0.75	0.01241	0.00123	10.10
Co High	0.75	5.91113	1.31256	4.50
Pb Med	1.19	0.03913	0.00906	4.32
As Low	0.72	0.01042	0.00727	1.43
Se High	0.64	0.60419	2.93091	0.21
As Med	0.72	0.00884	0.04790	0.18
As High	0.72	0.02326	1.19892	0.02

Table 5: Partition coefficients.

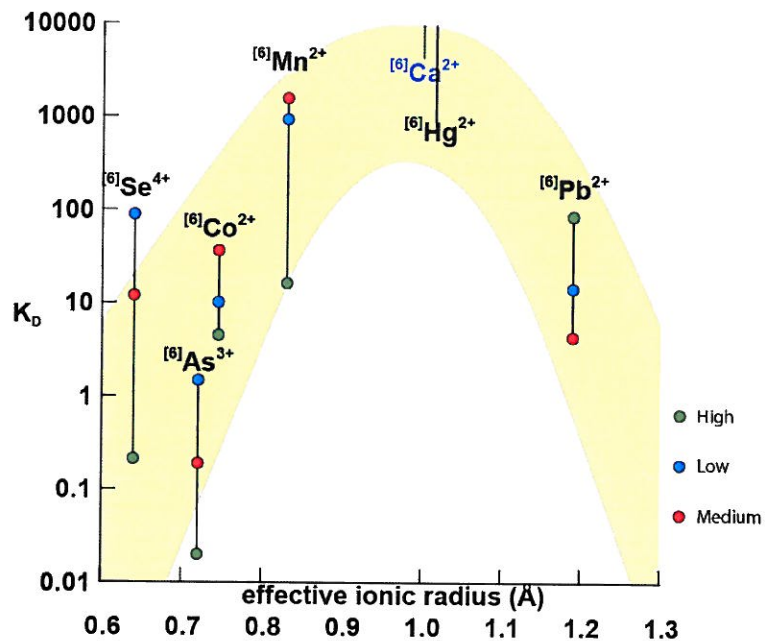


Figure 20: Partition coefficients plotted against effective ionic radius for octahedrally coordinated ions of interest. The shaded region is a visual approximation of the trend.

Discussion

The aqueous method for synthesizing calcite at low pH was successful in producing 50 μm -500 μm euhedral crystals of calcite. Examination with a petrographic microscope indicated that even masses of fine (sub-micron sized) powders present in most of the experimental runs were isotropic and therefore crystalline (and not amorphous CaCO_3) and XRD analyses indicated that the crystals that precipitated were mostly calcite with some vaterite and possibly some spherocobaltite in experiments grown with medium and high concentrations of cobalt. The removal of toxic trace metals from aqueous solutions via an aqueous calcite synthesis method was achieved with different degrees of success for different metals. In this section, the outcome of the different experiments, as seen by the different analytical techniques implemented on the samples, as well as the implications of these results for implementing a new decontamination protocol will be discussed.

The concentration of cobalt and manganese was reduced at all contaminant concentrations (high, medium and low), and for lead at high concentrations. In cobalt doped samples, there is approximately a 90% difference between the initial and final concentrations of cobalt in water, and a greater amount of cobalt in solid samples with respect to the blank. The difference in concentration is sufficient to hypothesize that cobalt has been successfully incorporated into calcite, with a calculated weight of cobalt in the solid samples of 5.9mg, 0.11 mg, and 0.012mg in of cobalt in the high, medium, and low concentration samples, respectively.

It is possible that the mechanism of the reduction in cobalt concentration in the liquids throughout the experiment includes the co-precipitation of spherocobaltite. The X-ray diffraction spectra for the cobalt samples contained spherocobaltite peaks but the

highest spherocobaltite and vaterite peaks overlap making a definitive observation of spherocobaltite difficult. Both minerals are likely to be present on the samples. On the one hand, vaterite was a likely component because it was present in the other samples, including crystals formed from solutions with low concentrations of cobalt; on the other hand, the sample could have had low concentrations of spherocobaltite, because of the high levels of cobalt added to the initial solution and the precipitation of spherical crystals that are pink to light purple in color. The X-ray Diffraction results do not provide an unequivocal answer about the co-precipitation of spherocobaltite.

The aqueous concentrations of manganese in the final liquid were reduced by more than 90% with respect to the initial concentrations for all contamination levels. The difference in manganese content is attributed to either the incorporation of Mn^{2+} in the Ca^{2+} site in calcite or the co-precipitation of a $(Ca,Mn)CO_3$ solid solution member with calcite. The levels of manganese were well above the detection limit and the background amounts, and the observed difference in manganese concentration can be quantified confidently.

The lead experiments had different results for different concentrations of lead. At low concentrations, 15ppb solutions, there was a modest reduction of the lead concentration in the solutions. The final concentrations of lead were below the EPA legal concentration limit, but cannot be confidently stated to be below the WHO standards. The background level of lead, the lead in the non-lead experiments, increases continually through time. The level of lead in the background lowers the credibility of modest decrease in lead content. The lead experiments with medium concentration, 150ppb, also showed a modest decrease in the concentration of lead. However, the lead content in the final

experiment solutions is much above both the EPA and the WHO contamination limits.

There is also a small increase in lead concentration between the day 5 value and the day 10 amounts. For lead at high concentrations there was a considerable reduction in concentration levels. At high concentration the background level of lead is also a small fraction of the total lead content, and the results are more robust. The difference in lead content is expected to be incorporated in calcite, but because of the high concentrations of lead in the background, it is difficult to confidently quantify the total incorporation of lead in calcite.

The selenium and arsenic concentrations in the final solutions were not always distinctly different from the initial concentrations. Selenium at high concentrations, 50ppm, is reduced to below 30ppm, although this is still considerably above the EPA and WHO drinking water standard. For both selenium and arsenic in none of the cases did the level of contamination consistently dropped to below the guideline maximum levels, one of the selenium experiments at low concentration had a final liquid concentration below the EPA standards; however, this result was not replicated by the other two samples. For both selenium and arsenic, the background concentration levels in the low and medium concentration samples were elevated but not for the high concentration levels.

The high concentration experiments have low background levels because the source of the additional trace metals are the relatively impure reagents; however, as the contribution of contaminants from the reagents remains constant for all the experiments, the contribution is the same in absolute terms but varies in relative terms as the concentration of contaminants in the initial solution changes by three orders of magnitude. In short, the starting materials (CaCl_2 and $(\text{NH}_4)_2\text{CO}_3$) used in these calcite synthesis

experiments contained significant concentrations of lead, arsenic, and selenium and this made it difficult to affectively gauge the incorporation of these ions into the growing calcite. It was not possible to confidently draw any conclusions about success of these experiments in reducing the levels of mercury at the lower concentrations (2ppb, 20ppb and 200ppb experiments), because of the very high detection limits and the lack of information about background levels of mercury in other samples. The levels of mercury at the highest concentration, however, are higher than the detection limit and show a slight decrease in mercury concentration from 20ppb to less than 15ppb. These values are well above the EPA and WHO drinking water safety standard.

Partition Coefficients

The partition coefficients were calculated based on the concentration of the solids obtained from the ICP-OES solid analysis and the final liquid concentration for the different ICP liquid runs (Figure 20). The general shape of the graph is similar to the predicted values from solving the Blundy and Wood (2003) equation. The maximum value, however, was not 1 but 10000. The partition coefficients were several orders of magnitude larger than those predicted (Figure 2).

As predicted, manganese was the most compatible element in calcite, then cobalt and lead are both similarly compatible. Selenium at low concentration has a higher partition coefficient than both cobalt or lead, however this might be due to anomalously high concentrations of selenium in the final solid. The concentration of the contaminant seems to change the partition coefficient, since for every element, the partition coefficients for different concentrations are orders of magnitude different. The way in which concentration affects the partition coefficient varies across the trace metals. The partition

coefficient of lead at high concentration is the highest among all lead samples, but this is the only case where the highest concentration of an element also has the highest coefficient. In the case of selenium and arsenic it is the samples at the lowest concentrations that have the highest partition coefficient. For manganese and cobalt, however, the samples at medium concentrations have the highest partition coefficient.

The lattice strain theory developed by Blundy and Wood (2003), explains that for each lattice site there is an ideal ion. The likeliness of a different ion incorporating into a specific lattice site is based on the ionic radius and charge of the ion of interest, as well as lattice specific parameters, like its Young's modulus (how difficult it is to deform the lattice to accommodate the ion) and the ideal lattice size [based on the ionic radius of the ideal ion] (Equation 2). A limitation of the Blundy and Wood (2003) model is that it does not account for alternative incorporation mechanisms, like sorption to the crystal surfaces or coprecipitation of end member carbonates including the possible precipitation of sphaerocobaltite. The initial crystallization of calcite probably approximates a pure substitution system; however, calcite grows in monomolecular lattice steps, and as it grows, it provides a fresh surface for the sorption of surface reactants (Lorens, 1981; Curti, 1999; Lashtanov 2007). The next step in this research is to calculate the predicted partition coefficients in a sorption dominated system and compare them with the values measured in this project and the Blundy and Wood (2003) calculated values.

Limitations to Implementation

The implementation potential of this method as it is very small because of the impurity of the calcium chloride reagents used. Even if the levels of cobalt and manganese or the high concentrations of lead were effectively reduced, the absolute levels of arsenic

would increase. It would still be possible to find a balance between affordable and contaminant free calcium solutions (even if the samples are not pure, they could contain secondary elements that are only harmful at very high levels, like sodium or magnesium).

Also, the use of ammonium carbonate as a reagent results in final levels of dissolved ammonium that were very high. While there is no guideline that regulates the amount of ammonium or ammonia (which can be often found with Ammonium depending on the pH of the water) in drinking water, high levels of ammonium can interfere with disinfectants, like chlorine, used at water treatments plants (Sawyer, 2008) and having 500ppm of ammonium might have negative aesthetic effects that influence the quality of drinking water (Sawyer, 2008). The presence of ammonium can be positive, since ammonium can be useful in promoting plant growth. A solution might be to change the source of carbonate from ammonium carbonate to sodium carbonate, which is also very soluble in water, or to use the ammonium from the final water for irrigation where high levels of ammonium might be an asset.

Another factor that will impact the implementation capabilities of this study is whether it can be done in several steps. The results for lead are particularly promising because (ignoring the effects of background) it is possible to reduce the contaminants to below the legal limit. The highest concentrations of lead, however, were too high even after a successful experiment. If the synthesis can be conducted in steps then it might be possible to reduce the levels of lead from 15ppm to below 15ppb in a couple of weeks with a two-step method.

Ideally, a similar aqueous synthesis method would be used to precipitate crystals in contaminated water and the solid crystals would be removed via filtration and then stored

in a suitable environment. An advantage of this system is that it does not rely of sludgy ponds for storing the separated heavy metals; however, given the relative instability of calcite (it can dissolve easily when exposed to liquids with low pH), it would be important to make arrangements for the long-term storage or transformation of the heavy metal doped calcite crystals.

Future Work

For future studies, it would be desirable to have a more frequent sampling protocol. For most elements there was not a substantial change between day 5 and day 10 solutions, but there was a substantial change between day 1 and day 5. If more samples are taken between day 0 and day 5 it might be possible to understand the rates of reaction better and even shorten the crystallization experiments to less than ten days. A blank sample also needs to be set up to analyzed with the ICP-OES, so that it is possible to develop a background level for mercury. Also, samples of different concentration ranges need to be studied to characterize the effect of concentration of the partition coefficient and to obtain the most effective metal concentration range for the experiments.

The current set of liquid samples will be analyzed with IC for major anions, including dissolved nitrate and nitrite. Also, the full set of ICP data will be processed and analyzed additional elements in the low, medium and high concentration ICP-OES analytical runs. The crystals will also be analyzed under Scanning Electron Microscope – Energy Dispersive Spectrometry to compare surface trace element concentration with total concentrations measured using the ICP-OES to examine the rate of surface adsorption versus crystal lattice incorporation.

Conclusions

The experiments had varying degrees of success in removing the desired trace metal contaminants from the aqueous solutions using this calcite synthesis to promote incorporation or co-precipitation. The samples for the solutions at day 10 had highly reduced levels of cobalt, and manganese at all concentrations as well as lead for the highest concentration experiments, when compared to the initial trace metal concentrations, at day 0. The study also had modest success rates with lead at medium and low concentration, selenium at the highest concentration, and mercury at the highest concentration. This method did show not; however, ameliorate the contamination levels for arsenic or selenium at the low and medium concentrations. The experiments showed unclear levels of success for mercury at the lower concentrations (very low, low and medium concentrations), and a slight decrease in mercury concentration at the highest initial concentration.

The implementation potential for this calcite synthesis as a decontamination tool is limited by the quality of the reagents and the high ammonium in the resulting water. The effectiveness of the removal of arsenic, lead and selenium was difficult to quantify because of the high levels of background concentrations, or the concentration of trace metals caused by the reagents (CaCl_2 and/or $(\text{NH}_4)_2\text{CO}_3$). Cleaner sources of calcium and carbonate would potentially increase the applicability of this method in lead decontamination, however, the effective removal of arsenic and selenium would still be limited. The effective removal of mercury hasn't been adequately characterized in this study; it is possible that ICP-OES is not an adequate analytical tool for measuring mercury

at concentrations below 1 ppm. A modification of this method could become an important tool in the removal of lead, cobalt and manganese from environmental water.

References

- Agnihotri, R., Mahuli, S. K., Chauk, S. S., & Fan, L. (1999). Influence of surface modifiers on the structure of precipitated calcium carbonate. *Industrial and Engineering Chemistry Research*, 38, 2283-2291.
- Agency for Toxic Substance & Disease Registry (2011). *Arsenic, Cobalt, Lead, Manganese, Mercury, Selenium*. Retrieved from: <http://www.atsdr.cdc.gov/>
- Aurelio, G., Fernández-Martínez, A., Cuello, G.J., Román-Ross, G., Alliot, I., & Charlet, L. (2010) Structural study of selenium ⁴⁺ substitution in calcite. *Chemical Geology*, 270, 249-256.
- Blundy, J., & Wood, B. (2003) Partitioning of trace elements between crystals and melts. *Earth and Planetary Science Letters*, 210, 383-397.
- Broker, R.A., Du, Z., Blundy, J.D., Kelley, S.P., Allan, N.L, Wood, B.J., Chamorro, E.M., Whartha, J-A, Purton, J.A. (2003) The 'zero charge' partitioning behavior of noble gases during mantle melting. *Nature*, 423, 738-741.
- Cai, G., Zhao, G., Wang, X., & Yu, S. (2010). Synthesis of polyacrylic acid stabilized amorphous calcium carbonate nanoparticles and their application for removal of toxic heavy metal ions in water. *Journal of Physical Chemistry C*, 114, 12948-12954.
- Chen, J., Wang, Y., Guo, F., Wang, X., & Zheng, C. (2000). Synthesis of nanoparticles with novel technology: High-gravity reactive precipitation. *Industrial and Engineering Chemistry Research*, 39, 948-954.
- Curti, E. (1999). Coprecipitation of radionuclide with calcite: estimation of partition coefficients based on a review of laboratory investigations and geochemical data. *Applied Geochemistry*, 14, 433-445.

- Davis, J.A., Fuller, C.C., & Cook, A.D. (1987) A model from trace metal sorption processes at the calcite surface: Adsorption of Cd^{2+} and subsequent solid solution formation. *Geochimica et Cosmochimica*, 51, 1477-1490.
- Donners, J. M., Heywood, B. R., Meijer, E. W., Nolte, R. J. M., & Sommerdijk, N.. (2002). Control over calcium carbonate phase formation by dendrimer/surfactant templates. *Chemistry - A European Journal*, 8, 2561-2567.
- Downs, R.T. (2006). The RRUFF Project: an integrated study of the chemistry, crystallography, Raman and infrared spectroscopy of minerals. *Program and Abstracts of the 19th General Meeting of the International Mineralogical Association in Kobe, Japan*. 003-13.
- Environmental Protection Agency (2011) *Revision to the unregulated contaminant monitoring regulation (UCMR 3)*. Retrieved from:
<https://federalregister.gov/a/2011-4641>
- Environmental Protection Agency (2009) *National Primary Drinking Water Regulations*. Retrieved from: <http://water.epa.gov/drink/contaminants/index.cfm#Primary>
- Fernelius, W.C. and Detling, K.D. (1934) Preparation of crystals of sparingly soluble salts. *Journal of Chemical Education*, 11, 176-178.
- Faatz, M., Gröhn, F., & Wegner, G. (2004). Amorphous calcium carbonate: Synthesis and potential intermediate in biomineralization. *Advanced Materials*, 16, 996-1000.
- García-Sánchez, A., & Álvarez-Ayuso, E. (2002) Sorption of Zn, Cd, Cr on calcite. Application to purification of industrial wasterwaters. *Minerals Engineering*, 15, 539-547.

- Gao, C., Dong, Y., Zhang, H., & Zhang, J. (2007) Utilization of distiller waste and residual mother liquor to prepare precipitated calcium carbonate. *Journal of Cleaner Production*, 15, 1419-1425.
- Graf D. L. (1961), Crystallographic tables for the rhombohedral carbonates. *American Mineralogist*, 46, 1283-1316. Retrieved from:
http://webmineral.com/jpowd/JPX/jpowd.php?target_file=Calcite.jpg
- Guo, X. , Liu, L., Wang, W. , Zhang, J., Wang, Y , & Yu, S.H. (2011). Controlled crystallization of hierarchical and porous calcium carbonate crystals using polypeptide type block copolymer as crystal growth modifier in a mixed solution. *Crystal Engineering Communication*, 3, 2054-2061.
- Gupta, H., & Fan, L. (2002). Carbonation-calcination cycle using high reactivity calcium oxide for carbon dioxide separation from flue gas. *Industrial and Engineering Chemistry Research*, 41, 4035-4042.
- Hay, M.B., Workman, R.K., & Manne, S. (2002). Mechanism of metal sorption on calcite: Composition mapping by Lateral Force Microscopy. *Langmuir*, 19, 3727-3740.
- Heberling, F., Denecke, M.A., & Bosbach, D. (2008) Neptunium(V) coprecipitation with calcite. *Environmental Science and Technology*, 42, 471-476.
- Hirai, T., Hariguchi, S., Komazawa, I., & Davey, R. J. (1997). Biomimetic synthesis of calcium carbonate particles in a pseudovesicular double emulsion. *Langmuir*, 13, 6650-6653.
- Kamhi, S.R. (1963). On the structure of vaterite, CaCO₃. *Acta Crystallographica*, 16, 770-772.
- Isopescu, R., Mihai, M., Capat, C., Olaru, A., Mateescu, C., & Dumitrescu, O. (2011). Modelling of calcium carbonate synthesis by gas-liquid reaction using CO₂ from flue gases. *Chemical Engineering Transactions*, 25, 713-718.

- Kelly, S.D., Rasbury E.T, Chattopadhyay, S., Kropf, A.J, & Kemner, K.M. (2006). Evidence of a stable uranyl site in ancient organic-rich calcite. *Environmental Science and Technology*, 40, 2262-2268.
- Lakshatanov, L.Z, & Stipp, S.L.S. (2007) Experimental study of nickel²⁺ interaction with calcite: Adsorption and coprecipitation. *Geochimical et Cosmochimica Acta*, 71, 3686-3697.
- Liu, L., He, D., Wang, G., & Yu, S. (2011). Bioinspired crystallization of CaCO₃ coatings on electrospun cellulose acetate fiber scaffolds and corresponding CaCO₃ microtube networks. *Langmuir*, 27, 7199-7206.
- Lorens, R. (1981). Sd, Cd, Mn and Co distribution coefficients in calcite as a function of calcite precipitation rate. *Geochimica et Cosmochimica Acta*, 45, 553-561.
- Mercury preservation techniques (2003). US Environmental Protection Agency. Retrieved from: <http://www.epa.gov/esd/factsheets/mpt.pdf>
- Morrison, J.M, Reimi, M.A., & Burns, P.C. Controlled nucleation and growth of calcite in an aqueous system (manuscript).
- Morse, J (1983). The kinetic of calcium carbonate dissolution and precipitation. In Reeder, R. and Ribbe, P. (Eds.), Carbonates: Mineralogy and chemistry. *Reviews in Mineralogy* (vol. 11). Mineralogical Society of America, Chantilly, Virginia.
- Naka, K., & Chujo, Y. (2001). Control of crystal nucleation and growth of calcium carbonate by synthetic substrates. *Chemistry of Materials*, 13, 3245-3259.
- Nordstrom D. K. (2004) Worldwide occurrences of arsenic in ground water. *Science* 296, 2143-2144.

- Ohara, M., & Reid, R.C. (1973) Modeling crystal growth rates from solution. *Prentice-Hall International Series*, 272.
- Reeder, R. (1983a). Preface. In Reeder, R. and Ribbe, P. (Eds.), Carbonates: Mineralogy and chemistry. *Reviews in Mineralogy* (Vol.11, pp. 1-48). Mineralogical Society of America, Chantilly, Virginia.
- Reeder, R. (1983b) Crystal chemistry of the rhombohedral carbonates. In Reeder, R. and Ribbe, P. (Eds.), Carbonates: Mineralogy and chemistry. *Reviews in Mineralogy* (Vol.11, pp. 1-48). Mineralogical Society of America, Chantilly, Virginia.
- Rickard, D.T., & Sjöberg, L. (1983) Mixed kinetic control of calcite dissolution rates. *American Journal of Science*, 283, 815-830.
- Sawyer, J. (2008). Surface Waters: Ammonium is not Ammonia – Part TWO. *Integrated Crop Management News*. Retrived from:
<http://www.extension.iastate.edu/CropNews/2008/0502JohnSawyer.htm>.
- Shannon, R.D. (1976), Revised effective ionic radii and systematic studies of interatomic distances in halides and chalcogenides, *Acta Crystallographica*, 32, 751-767.
- Skogerboe, R. K., & Grant, C. L. (1970). Comments on the definitions of the terms sensitivity and detection limit. *Spectroscopy Letters*, 3, 8-9.
- Sposito, G., & Weber, J. (1986). Sorption of trace metals by humic materials in soils and natural waters. *Critical Reviews in Environmental Control*, 16, 193-229.
- Sun, B., Wang, X. M., Chen, J.M., Chu, G.W., Chen, J.F., & Shao, L. (2011) Synthesis of nano-CaCO₃ by simultaneous absorption of CO₂ and NH₃ into CaCl₂ solution in a rotating packed bed. *Chemical Engineering Journal*, 168, 731-736.

- Sø, H., Postma, D., Jakobsen, R., Larsen, F. (2008). Sorption and desorption of arsenate and arsenite on calcite. *Geochimica et Cosmochimica Acta*, 72, 5871-5884.
- Veizer, J. (1983) Trace elements and isotopes in sedimentary carbonates. In Reeder, R. and Ribbe, P. (Eds.), Carbonates: Mineralogy and chemistry. *Reviews in Mineralogy* (Vol.11). Mineralogical Society of America, Chantilly, Virginia.
- Wakita, H., & Kinoshita, S. (1985). Growth of tiny calcite single crystals in an aqueous solution. *Journal of Crystal Growth*, 71, 807-809.
- Warren, L.A., Maurice, P.A., Parmar, N., & Ferris, F.G. (2001) Microbially mediated calcium carbonate precipitation: Implications for interpreting calcite precipitation and for solid-phase capture of inorganic contaminants. *Geomicrobiology Journal*, 18, 93-115.
- West Virginia Department of Environmental Protection Water Resources (2011). Requirements Governing Water Quality Standards. Retrieved from:
<http://apps.sos.wv.gov/adlaw/csr/readfile.aspx?DocId=22316&Format=PDF>
- World Health Organization. (2011) *Guidelines for Drinking-water Quality*, 4th ed. Retrieved from: http://whqlibdoc.who.int/publications/2011/9789241548151_eng.pdf
- Xu, G., Yao, N., Aksay, I. A., & Groves, J. T. (1998). Biomimetic synthesis of macroscopic-scale calcium carbonate thin films. evidence for a multistep assembly process. *Journal of the American Chemical Society*, 120, 11977-11985.
- Zachara, J.M., Kittrick, J.A., Dake, L.S., & Harsh, J.B. (1989) Solubility and surface spectroscopy of zinc precipitates on calcite. *Geochimica et Cosmochimica Acta*, 53, 9-19.
- Zachara, J.M, Cowan, C.E., & Resch, C.T. (1991) Sorption of divalent metals on calcite. *Geochemica et Cosmochimica Acta*, 55, 1549-1562.